

NOT ALL PROMPTS ARE MADE EQUAL: PROMPT-BASED PRUNING OF TEXT-TO-IMAGE DIFFUSION MODELS

Anonymous authors

Paper under double-blind review

ABSTRACT

Text-to-image (T2I) diffusion models have demonstrated impressive image generation capabilities. Still, their computational intensity prohibits resource-constrained organizations from deploying T2I models after fine-tuning them on their internal *target* data. While pruning techniques offer a potential solution to reduce the computational burden of T2I models, static pruning methods use the same pruned model for all input prompts, overlooking the varying capacity requirements of different prompts. Dynamic pruning addresses this issue by utilizing a separate sub-network for each prompt, but it prevents batch parallelism on GPUs. To overcome these limitations, we introduce Adaptive Prompt-Tailored Pruning (APTP), a novel prompt-based pruning method designed for T2I diffusion models. Central to our approach is a *prompt router* model, which learns to determine the required capacity for an input text prompt and routes it to an architecture code, given a total desired compute budget for prompts. Each architecture code represents a specialized model tailored to the prompts assigned to it, and the number of codes is a hyperparameter. We train the prompt router and architecture codes using contrastive learning, ensuring that similar prompts are mapped to nearby codes. Further, we employ optimal transport to prevent the codes from collapsing into a single one. We demonstrate APTP’s effectiveness by pruning Stable Diffusion (SD) V2.1 using CC3M and COCO as *target* datasets. APTP outperforms the single-model pruning baselines in terms of FID, CLIP, and CMMD scores. Our analysis of the clusters learned by APTP reveals they are semantically meaningful. We also show that APTP can automatically discover previously empirically found challenging prompts for SD, *e.g.*, prompts for generating text images, assigning them to higher capacity codes.

1 INTRODUCTION

In recent years, diffusion models (Sohl-Dickstein et al., 2015; Ho et al., 2020; Song & Ermon, 2019; Song et al., 2021b) have revolutionized generative modeling. For instance, modern Text-to-Image (T2I) diffusion models (Adobe FireFly, 2023; Midjourney, 2023; Betker et al., 2023) like Stable Diffusion (Rombach et al., 2022; Podell et al., 2024) have achieved remarkable success in generating realistic images (Nichol et al., 2021; Saharia et al., 2022; Ramesh et al., 2022) and editing them (Kim et al., 2022; Hertz et al., 2022; Zhang et al., 2023b). Consequently, their integration into various applications is of great interest. However, the sampling process of T2I diffusion models is slow and computationally intensive, making them expensive to deploy on GPU clouds for a large number of users and preventing their utilization on edge devices. Thus, reducing the computational cost of T2I models is essential prior to serving them.

Two orthogonal factors underlie the sampling cost of T2I diffusion models: their large number of denoising steps and their parameter-heavy backbone architectures. Most acceleration methods for T2I models reduce the computation per sampling step or skip steps using techniques like distillation (Meng et al., 2023; Salimans & Ho, 2022; Habibian et al., 2023) and improved noise schedules (Song et al., 2021a; Nichol & Dhariwal, 2021). Other ideas address the second factor and propose efficient architectures for T2I models. Architecture modification methods (Zhao et al., 2023; Kim et al., 2023) modify the U-Net (Ronneberger et al., 2015) of Stable Diffusion (SD) (Rombach et al., 2022) to reduce its parameters and FLOPs while preserving performance. Still, they only provide a few

054
055
056
057
058
059
060
061
062
063
064
065
066
067
068
069
070
071
072
073
074
075
076
077
078
079
080
081
082
083
084
085
086
087
088
089
090
091
092
093
094
095
096
097
098
099
100
101
102
103
104
105
106
107

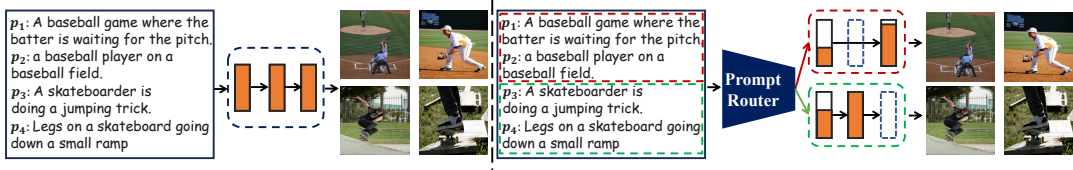


Figure 1: **Overview:** We prune a text-to-image diffusion model like Stable Diffusion (left) into a mixture of efficient experts (right) in a prompt-based manner. Our prompt router *routes* distinct types of prompts to different experts, allowing experts’ architectures to be separately specialized by removing layers or channels.

architectural configurations, and generalizing their design choices to new compute budgets or datasets is highly non-trivial. Search-based methods (Li et al., 2024; Liu et al., 2023a) search for an efficient architecture (Li et al., 2024) or an efficient mixture (Liu et al., 2023a) of pretrained T2I models in a model zoo. Yet, evaluating each action in the search process and gathering a model zoo of T2I models are both extremely costly, making search methods impractical in resource-constrained scenarios.

The efficient architecture design methods (Zhao et al., 2023; Kim et al., 2023; Li et al., 2024) have shown promise, but they aim to develop ‘one-size-fits-all’ architectures for *all* applications. We argue that this approach is misaligned with the common practice for two reasons: 1) Organizations typically fine-tune pretrained T2I models (*e.g.*, SD) on their proprietary *target* data and deploy the resulting model for their specific application. They prioritize performance on their *target* data distribution while meeting their computation budget, and the trade-off between efficiency and performance can vary depending on the complexity of the *target* dataset between organizations. 2) Verifying the validity of each design choice on large-scale datasets used in one-size-fits-all methods is costly and slow to iterate, making them impractical.

Model pruning (Cheng et al., 2023) can reduce a model’s computational burden to any desired budget with significantly less effort than designing (Zhao et al., 2023; Kim et al., 2023) or searching (Li et al., 2024) for efficient architectures. Still, T2I models have unique characteristics making existing pruning techniques unsuitable for them. Static pruning methods are input-agnostic and use the same pruned model for all inputs, but distinct prompts of T2I models may require different model capacities. Dynamic pruning employs a separate model for each input sample, but it cannot benefit from batch-parallelism in modern hardware like GPUs and TPUs.

In this paper, we introduce Adaptive Prompt-Tailored Pruning (AFTP), a novel prompt-based pruning method for T2I diffusion models. AFTP prunes a T2I model pretrained on a large-scale dataset (*e.g.*, SD) using a smaller *target* dataset given a desired compute budget. It tackles the challenges of static and dynamic pruning methods for T2I models by training a *prompt router* module along with a set of *architecture codes*. The prompt router learns to route an input prompt to an architecture code, determining the sub-architecture, called *expert*, of the T2I model to use. Each expert specializes in generating images for the prompts assigned to it by the prompt router (Fig. 1), and the number of experts is a hyperparameter. We train the prompt router and architecture codes using a contrastive learning objective that regularizes the prompt router to select similar architecture codes for similar prompts. In addition, we employ optimal transport to diversify the architecture codes and the resulting experts’ budgets, allowing deploying them on hardware with varying capabilities. We take CC3M (Sharma et al., 2018) and MS-COCO (Lin et al., 2014) as the *target* datasets and prune Stable Diffusion V2.1 (Rombach et al., 2022) using AFTP in our experiments. AFTP outperforms the single-model pruning baselines, and we show that our prompt router learns to group the input prompts into semantic clusters. Further, our analysis demonstrates that AFTP can automatically discover challenging prompts for SD, such as prompts for generating text images, found empirically by prior work (Chen et al., 2024; Yang et al., 2024). We summarize our contributions as follows:

- We introduce AFTP, a novel prompt-based pruning method for T2I diffusion models. It is more suitable than static pruning for T2I models as it is not input-agnostic. In addition, AFTP enables batch parallelism on GPUs, which is not possible with dynamic pruning.
- AFTP trains a prompt router and a set of architecture codes. The prompt router maps an input prompt to an architecture code. Each architecture code resembles a pruned sub-architecture expert of the T2I model, specialized in handling certain types of prompts assigned to it.

- We develop a framework to train the prompt router and architecture codes using contrastive learning and employ optimal transport to diversify the architecture codes and their corresponding sub-architectures’ computational requirements, given a desired compute budget.

2 RELATED WORK

Several works have addressed improving the architectural efficiency of diffusion models, which is our paper’s primary focus. **Multi-expert** (Lee et al., 2024; Zhang et al., 2023a; Liu et al., 2023a; Pan et al., 2024; Xue et al., 2023) methods employ several models each responsible for an interval of diffusion model’s denoising process. These methods design expert model architectures (Lee et al., 2024; Zhang et al., 2023a; Xue et al., 2023), train several models with varying capacities from scratch (Liu et al., 2023a), or utilize existing pretrained models (Liu et al., 2023a; Pan et al., 2024). However, pretrained experts may not be available, and training several models from scratch, as done by multi-expert methods, is prohibitively expensive. **Architecture Design** (Zhao et al., 2023; Yang et al., 2023a; Kim et al., 2023) approaches redesign the U-Net architecture (Ronneberger et al., 2015) of diffusion models to enhance its efficiency. MobileDiffusion (Zhao et al., 2023) does so using empirical heuristics derived from performance metrics on MS-COCO (Lin et al., 2014). BK-SDM (Kim et al., 2023) removes some blocks from the SD’s U-Net and applies distillation (Hinton et al., 2015) to train the pruned model. Spectral Diffusion (Yang et al., 2023a) introduces a wavelet gating operation and performs frequency domain distillation. Yet, generalizing heuristics and design choices of the architecture design methods to other tasks and compute budgets is non-trivial. Alternatively, SnapFusion (Li et al., 2024) searches for an efficient architecture for T2I models. Yet, evaluating each action in the search process requires 2.5 A100 GPU hours, making it costly in practice. Finally, SPDM (Fang et al., 2023) estimates the importance of different weights using Taylor expansion and removes the low-scored ones. Despite their promising results, all these methods are ‘static’ in that they obtain an efficient model and utilize it for *all* inputs. This is sub-optimal for T2I models as input prompts may vary in complexity, demanding different model capacity levels. Our method differs from existing approaches by introducing a prompt-based pruning technique for T2I models. It is the first method that allocates computational resources to prompts based on their individual complexities while ensuring optimal utilization and batch-parallelizability. We refer to Appendix B for a detailed review of related work, [with more focus on sampling efficiency studies that are orthogonal to our approach.](#)

3 METHOD

We introduce a framework for prompt-based pruning of T2I diffusion models termed Adaptive Prompt-Tailored Pruning (ATPT). ATPT prunes a T2I model pretrained on large-scale datasets (*e.g.*, Stable Diffusion (Rombach et al., 2022)) using a smaller *target* dataset. This approach mirrors the common practice where organizations fine-tune pretrained T2I models on their internal proprietary data and deploy the resulting model for their customers. The core component of ATPT is a *prompt router* that learns to map an input prompt to an *architecture code* during the pruning process. Each architecture code corresponds to a specialized *expert* model, which is a sub-network of the T2I model. We train the prompt router and architecture codes in an end-to-end manner. After the pruning phase, ATPT fine-tunes each specialized model using samples from the target dataset assigned to it by the prompt router. We elaborate on the components of ATPT in the following subsections.

3.1 BACKGROUND

Given an input text prompt, text-to-image (T2I) diffusion models generate a corresponding image by iteratively denoising a Gaussian noise (Ho et al., 2020; Song & Ermon, 2019; Sohl-Dickstein et al., 2015). They achieve this by training a denoising model, $\epsilon(\cdot; \theta)$, parameterized by θ . For a given training image-text pair $(x_0, p) \sim \mathcal{P}$, T2I models define a forward diffusion process, progressively adding Gaussian noise to the initial image x_0 over T steps. This process is defined as $q(x_t|x_0) = \mathcal{N}(x_t; \sqrt{\bar{\alpha}_t}x_0, (1 - \bar{\alpha}_t)I)$, where $\bar{\alpha}_t$ is the forward noise schedule parameter, typically chosen such that $q(x_t|x_0) \rightarrow \mathcal{N}(0, I)$ as $t \rightarrow T$. T2I models are trained using the variational evidence lower bound (ELBO) objective (Ho et al., 2020):

162
163
164
165
166
167
168
169
170
171
172
173
174
175
176
177
178
179
180
181
182
183
184
185
186
187
188
189
190
191
192
193
194
195
196
197
198
199
200
201
202
203
204
205
206
207
208
209
210
211
212
213
214
215

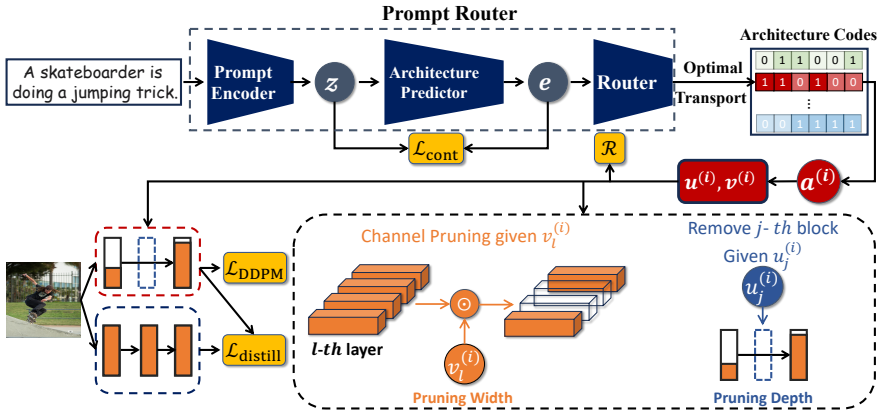


Figure 2: **Our pruning scheme.** We train our prompt router and the set of architecture codes to prune a text-to-image diffusion model into a mixture of experts. The prompt router consists of three modules. We use a Sentence Transformer (Reimers & Gurevych, 2019) as our prompt encoder to encode the input prompt into a representation z . Then, the architecture predictor transforms z into the architecture embedding e that has the same dimensionality as architecture codes. Finally, the router routes the embedding e into an architecture code $a^{(i)}$. We use optimal transport to evenly assign the prompts in a training batch to the architecture codes. The architecture code $a^{(i)} = (u^{(i)}, v^{(i)})$ determines pruning the model’s width and depth. We train the prompt router’s parameters and architecture codes in an end-to-end manner using the denoising objective of the pruned model $\mathcal{L}_{\text{DDPM}}$, distillation loss between the pruned and original models $\mathcal{L}_{\text{distill}}$, average resource usage for the samples in the batch \mathcal{R} , and contrastive objective $\mathcal{L}_{\text{cont}}$, encouraging embeddings e preserving semantic similarity of the representations z .

$$\mathcal{L}_{\text{DDPM}}(\theta) = \mathbb{E}_{\substack{(x_0, p) \sim \mathcal{P} \\ t \sim [1, T] \\ \epsilon \sim \mathcal{N}(0, I) \\ x_t \sim q(x_t | x_0)}} \|\epsilon(x_t, p, t; \theta) - \epsilon\|^2 \tag{1}$$

T2I models sample an image starting from a Gaussian noise $x_T \sim \mathcal{N}(0, I)$ and denoising it using the trained denoising model. We refer to appendix for a thorough review of diffusion models.

3.2 PROMPT ROUTER AND ARCHITECTURE CODES

Our approach prunes a diffusion model into a *Mixture of Experts*, where each expert specializes in handling a distinct group of prompts with different complexities. Each expert corresponds to a unique sub-network $a^{(i)} \in \mathbb{R}^D$, where D represents the total number of prunable units in the T2I model. These sub-networks are optimized to efficiently process their assigned prompt groups while maintaining high performance. To assign prompts to the appropriate expert sub-network, we design a *prompt router model* comprising three key components:

1. **Prompt Encoder:** This module encodes input prompts into semantically meaningful embeddings. Prompts with similar semantics are mapped to embeddings that are close in the embedding space, ensuring that similar prompts are routed to similar sub-networks.
2. **Architecture Predictor:** The encoded prompt embeddings are further transformed into architecture embeddings e . This step bridges the gap between the high-level semantics of prompts and the architectural configurations needed to process them efficiently.
3. **Router Module:** The architecture embeddings e are finally mapped to specific architecture codes a , which define the structure of the sub-network (expert) that will handle the prompt.

The remainder of this section provides detailed descriptions of how each component functions and contributes to the overall pruning and routing process.

We employ our prompt router to determine the specialized sub-network of the T2I model to be used for a given input prompt. Specifically, we denote our prompt router with the function $f_{\text{PR}}(\cdot; \eta, \mathcal{A})$, parameterized by η , which maps an input prompt p to an architecture code a :

216
217
218
219
220
221
222
223
224
225
226
227
228
229
230
231
232
233
234
235
236
237
238
239
240
241
242
243
244
245
246
247
248
249
250
251
252
253
254
255
256
257
258
259
260
261
262
263
264
265
266
267
268
269

$$a = f_{\text{PR}}(p; \eta, \mathcal{A}) \tag{2}$$

We define the set of learnable architecture codes as $\mathcal{A} = \{a^{(i)}\}_{i=1}^N$, where N is a hyperparameter. Also, $a^{(i)} \in \mathbb{R}^D$, with D being the number of prunable width and depth units in the T2I model. Given a desired constraint T_d on the total compute budget (latency, MACs, etc.) for the prompts in the target dataset, we train the prompt router’s parameters η and architecture codes in \mathcal{A} to obtain a set of expert models. These experts are specialized, efficient, and performant sub-networks of the T2I model, as determined by the architecture codes. As illustrated in Fig. 2, the prompt router consists of a prompt encoder, an architecture predictor, and a router module. We provide details of these components in the following subsections and present our pruning objective in Eq. 15.

3.2.1 PROMPT ENCODER AND ARCHITECTURE PREDICTOR

Our primary intuition in designing the prompt router is that it should route semantically similar prompts to similar sub-networks of a T2I model. Accordingly, we use a pretrained frozen Sentence Transformer model (Reimers & Gurevych, 2019) as our prompt encoder module. It can effectively encode input prompts p into semantically meaningful embeddings z :

$$z = f_{\text{PE}}(p) \tag{3}$$

$f_{\text{PE}}(\cdot)$ is the prompt encoder. We do not explicitly show the prompt encoder’s parameters as we do not train them in our pruning method. The Sentence Transformer can encode semantically similar prompts to nearby embeddings and distant from dissimilar ones. We leverage this property in our framework (Eq. 13) to ensure the prompt router maps similar prompts to similar architecture codes.

The architecture predictor module transforms prompt embeddings z into architecture embeddings e :

$$e = f_{\text{AP}}(z; \eta) \tag{4}$$

η denotes the parameters of the architecture predictor $f_{\text{AP}}(\cdot)$, implemented with a single feed-forward layer (more details in Appendix D). The embeddings e have the same dimensionality as the architecture codes a .

3.2.2 ROUTER

The router module takes an architecture embedding e and routes it to an architecture code $a \in \mathcal{A}$. A straightforward way to implement the router is to map an input embedding e to its nearest architecture code in \mathcal{A} . However, we found that this approach may lead to the collapse of architecture codes, as they could converge to a single code that meets the desired compute budget T_d with a relatively decent performance, causing the prompt router to route all input prompts to it.

To tackle this challenge, we employ optimal transport in our router module during the pruning phase. Formally, let $E = [e_1, \dots, e_B]$ represent B architecture embeddings in a training batch, and $A = [a^{(1)}, \dots, a^{(N)}]$ represent the N codes. The goal is to find an assignment matrix $Q = [q_1, \dots, q_B]$ that maximizes the similarity between architecture embeddings and their assigned architecture codes:

$$\max_{Q \in \mathcal{Q}} \text{Tr}(Q^T A^T E) + \epsilon H(Q) \tag{5}$$

H is an entropy term $H(Q) = -\sum_{i,j} q_{ij} \log(q_{ij})$ and ϵ is the regularization strength. It has been shown (YM. et al., 2020; Caron et al., 2020) that high values of ϵ lead to a uniform assignment matrix Q , causing all codes in A to collapse to a single code. Thus, we set ϵ to a small value. Further, we impose an equipartition (YM. et al., 2020) constraint on Q so that architecture embeddings in a batch are assigned equally to architecture codes:

$$\mathcal{Q} = \{Q \in \mathbb{R}_+^{N \times B} \mid Q \mathbf{1}_B = \frac{1}{N} \mathbf{1}_N, Q^T \mathbf{1}_N = \frac{1}{B} \mathbf{1}_B\} \tag{6}$$

Here, $\mathbf{1}_{\{B,N\}}$ are vectors of ones with length B and N , respectively. These constraints enforce that, on average, $\frac{B}{N}$ embeddings are assigned to an architecture code per training batch, thereby ensuring

that each architecture code gets enough samples for training. The optimal transport problem in Eq. 5 with the constraints in Eq. 6 can be solved using the fast version (Cuturi, 2013) of the Sinkhorn-Knopp algorithm and the solution has the normalized exponential matrix form (Cuturi, 2013):

$$Q^* = \text{diag}(m) \exp\left(\frac{A^T E}{\epsilon}\right) \text{diag}(n) \quad (7)$$

Here, m and n are renormalization vectors that can be calculated using a few iterations of the Sinkhorn-Knopp algorithm. With ϵ set to a small value, the matrix BQ^* will have columns that are close to one-hot vectors, which we use to assign the architecture embeddings to the architecture codes. In summary, the router module’s function during the pruning process is:

$$a = f_R(e, \mathcal{A}; Q^*) \quad (8)$$

After the pruning stage, the trained router simply routes an input architecture embedding to an architecture code with the highest cosine similarity. We provide the definition of f_R in Appendix D.2.

3.3 PRUNING

We divide each architecture code $a^{(i)} \in \mathcal{A}$ into two sub-vectors $a^{(i)} = (u^{(i)}, v^{(i)})$. We utilize the vectors $u^{(i)}$ and $v^{(i)}$ to prune the depth layers and determine widths of the layers, respectively.

A simple approach to prune the width of a layer (a depth layer) is to use binary vectors $v^{(i)}$ ($u^{(i)}$), indicating whether the channels (layers) should be pruned. Yet, doing so is not differentiable, and one needs to solve a discrete optimization problem to find the optimal binary vectors. Instead, we employ soft vectors $\mathbf{v}^{(i)}$ ($\mathbf{u}^{(i)}$) that are continuous and differentiable for pruning. We calculate them as:

$$\mathbf{v}^{(i)} = \text{sigmoid}\left(\frac{v^{(i)} + g_v}{\gamma}\right), \quad \mathbf{u}^{(i)} = \text{sigmoid}\left(\frac{u^{(i)} + g_u}{\gamma}\right) \quad (9)$$

$g_{\{u,v\}} \sim \text{Gumbel}(0, 1)$ represents a noise vector sampled from the Gumbel distribution (Gumbel, 1954), and γ is the temperature. This formulation, known as the Gumbel-sigmoid reparameterization (Jang et al., 2017; Maddison et al., 2017), is a differentiable approximation of sampling from Bernoulli distributions with parameters $\text{sigmoid}(v^{(i)})$ and $\text{sigmoid}(u^{(i)})$. When the temperature γ is set appropriately, the vectors $\mathbf{v}^{(i)}$ and $\mathbf{u}^{(i)}$ will be close to binary vectors, and we use them for pruning the layers’ width and depth layers. Assuming $\mathbf{v}^{(i)} = [\mathbf{v}_l^{(i)}]_{l=1}^L$ where L is the number of the model’s layers, we prune the width of the l -th layer as:

$$\widehat{\mathcal{F}}_l = \mathcal{F}_l \odot \mathbf{v}_l^{(i)} \quad (10)$$

In this equation, \mathcal{F}_l represents feature maps of the l -th layer, and \odot is the element-wise multiplication. We prune the channels of the convolution layers in the ResBlocks (He et al., 2016), attention heads in the Transformer layers (Vaswani et al., 2017), and the channels of the feed-forward layers in the Transformer layers.

In a similar manner, we apply the vectors $\mathbf{u}^{(i)} = [\mathbf{u}_j^{(i)}]_{j=1}^M$ (where M is the number of depth layers that we prune) for pruning the model’s depth. Specifically, we prune the j -th depth layer f_j as:

$$\widehat{\mathcal{F}}_j = \mathbf{u}_j^{(i)} f_j(\mathcal{F}_{j-1}) + (1 - \mathbf{u}_j^{(i)}) \mathcal{F}_{j-1} \quad (11)$$

\mathcal{F}_{j-1} denotes the previous layer’s feature maps. The granularity of our depth pruning is a ResBlock or a Transformer layer in the U-Net of the T2I model. We provide more details in Appendix D.3. In summary, we employ the architecture vectors $\mathbf{a}^{(i)} = (\mathbf{v}^{(i)}, \mathbf{u}^{(i)})$ to prune the T2I model.

3.3.1 TRAINING THE PROMPT ROUTER AND ARCHITECTURE CODES

We jointly train the prompt router and architecture codes in an end-to-end manner, guiding the prompt router to map similar prompts to similar architecture codes. In addition, we regularize the architecture codes to correspond to performant sub-networks of the T2I model, be diverse, and adhere to the desired compute budget T_d on aggregate.

Contrastive Training. Given a training batch with B prompts, we compute their prompt embeddings z (Eq. 3) and architecture embeddings e (Eq. 4). Then, we calculate architecture vectors \mathbf{e}' :

$$\mathbf{e}' = \text{sigmoid}\left(\frac{e + g}{\gamma}\right) \quad (12)$$

where γ and g have the same definitions as Eq. 9. We define the cosine similarity of two vectors as $\text{sim}(\mathbf{m}, \mathbf{n}) = \mathbf{m}^T \mathbf{n} / \|\mathbf{m}\| \cdot \|\mathbf{n}\|$, and we use the following objective to train the architecture predictor:

$$\mathcal{L}_{\text{cont}}(\eta) = \frac{1}{B^2} \sum_{i=1}^B \sum_{j=1}^B r_{i,j} \log(s_{i,j}) + (1 - r_{i,j}) \log(1 - s_{i,j}) \quad (13)$$

$$r_{i,j} = \frac{\exp(\text{sim}(z_i, z_j)/\tau)}{\sum_{k=1}^B \exp(\text{sim}(z_i, z_k)/\tau)}, \quad s_{i,j} = \frac{\exp(\text{sim}(\mathbf{e}'_i, \mathbf{e}'_j)/\tau)}{\sum_{k=1}^B \exp(\text{sim}(\mathbf{e}'_i, \mathbf{e}'_k)/\tau)} \quad (14)$$

τ is a temperature parameter. Eq. 13 regularizes the architecture predictor to map representations z to the regions of the space of the architecture embeddings e such that their corresponding architecture vectors \mathbf{e}' maintain the similarity between the prompts. Note that we do not actually use the architecture vectors \mathbf{e}' to prune the model (Sec. 3.2.2, 3.3). Yet, we apply our contrastive regularization to the vectors \mathbf{e}' instead of embeddings e . This design choice is a result of our observation that applying $\mathcal{L}_{\text{cont}}$ to embeddings e may not lead to diverse architecture vectors $\mathbf{a}^{(i)} = (\mathbf{v}^{(i)}, \mathbf{u}^{(i)})$ that we use for pruning (Sec. 3.3). For instance, embeddings e (and their nearby architecture codes a) can be distributed in the embedding space (before Gumbel-Sigmoid estimation), but all be in saturation regions of the sigmoid function (Eqs. 9, 12), resulting in similar architecture vectors \mathbf{e}' and $\mathbf{a}^{(i)}$.

In contrast, Eq. 13 implicitly diversifies the architecture vectors $\mathbf{a}^{(i)}$. The reason is that the router routes embeddings e to codes a (Eq. 8) that have high similarity with each other (Eq. 7). Also, Eq. 13 distributes embeddings e in the space of the architecture embeddings such that the architecture vectors \mathbf{e}' become similar (different) for similar (dissimilar) prompts. As the vectors \mathbf{e}' and $\mathbf{a}^{(i)}$ are calculated in a similar manner (Eqs. 9, 12), the diversity of vectors \mathbf{e}' implies the same for vectors $\mathbf{a}^{(i)}$.

Assuming $B^{(i)}$ samples get routed to the architecture code $a^{(i)}$ in a training batch ($\sum_i B^{(i)} = B$), we train the prompt router and the architecture codes using the following objective:

$$\min_{\eta, \mathcal{A}} \mathcal{L} = \left[\frac{1}{N} \sum_{i=1}^N \left[\frac{1}{B^{(i)}} \sum_{j=1}^{B^{(i)}} [\mathcal{L}_{\text{DDPM}}(x_j^{(i)}, p_j^{(i)}; a^{(i)}) + \lambda_{\text{distill}} \mathcal{L}_{\text{distill}}(x_j^{(i)}, p_j^{(i)}; a^{(i)})] \right] \right] + \lambda_{\text{res}} \mathcal{R}(\hat{T}(\mathcal{A}), T_d) + \lambda_{\text{cont}} \mathcal{L}_{\text{cont}}(\eta) \quad (15)$$

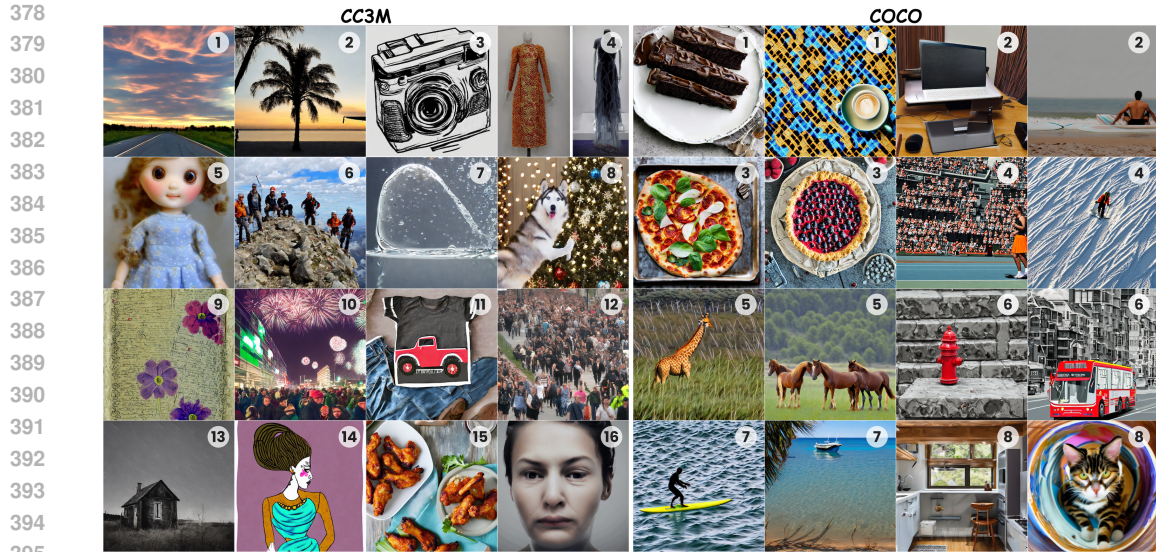
$\mathcal{L}_{\text{DDPM}}((x_j^{(i)}, p_j^{(i)}; a^{(i)})$ denotes the denoising objective for the sample $(x_j^{(i)}, p_j^{(i)})$ routed to sub-network chosen by the architecture code $a^{(i)}$. $\mathcal{R}(\hat{T}(\mathcal{A}), T_d)$ regularizes the weighted average of the MACs used by architecture codes ($\hat{T}(\mathcal{A}) = \sum_i \frac{B^{(i)}}{B} [\hat{T}(a^{(i)})]$) to be close to T_d . We define $\mathcal{R}(x, y) = \log(\max(x, y) / \min(x, y))$, and $\{\lambda_{\text{distill}}, \lambda_{\text{res}}, \lambda_{\text{cont}}\}$ are hyperparameters. Finally, $\mathcal{L}_{\text{distill}}$ is the distillation objective (Kim et al., 2023) regularizing the pruned model having similar outputs to the original one. We refer to Appendix D.4 for more details about our distillation objective.

3.4 FINE-TUNING THE PRUNED EXPERT MODELS

After the pruning stage, we use the learned architecture codes to prune the T2I model into our experts. Then, we fine-tune experts using samples routed to them. We use the same training objective as the pretraining stage while adding distillation to fine-tune experts and refer to Appendix D.5 for more details. At test time, our trained prompt router routes an input prompt to one of the experts, and we use the expert to generate an image for it.

4 EXPERIMENTS

We use Conceptual Captions 3M (CC3M) (Sharma et al., 2018) and MS-COCO (Lin et al., 2014) as our *target* datasets to prune the Stable Diffusion (SD) V2.1 model to demonstrate APTP’s effectiveness. On CC3M, we prune the model with Base: (0.85 MACs, 16 experts) and Small: (0.66



396 Figure 3: Samples of the APTP-Base experts after pruning the Stable Diffusion V2.1 using
397 CC3M Sharma et al. (2018) and COCO Lin et al. (2014) as the *target* datasets. Expert IDs are
398 shown on the top right of images. (See Table 7 for prompts)
399
400

401 MACs, 8 experts) configurations. On MS-COCO, we perform Base: (0.78 MACs, 8 experts) and
402 Small: (0.64 MACs, 8 experts) pruning settings. We set $(\lambda_{\text{distill}}, \lambda_{\text{res}}, \lambda_{\text{cont}}) = (0.2, 2.0, 100)$ (Eq. 15)
403 and the temperature τ (Eq. 14) to 0.03. We evaluate all models with FID (Heusel et al., 2017),
404 CLIP (Hessel et al., 2021), and CMMD (Jayasumana et al., 2023) scores using 14k samples in the
405 validation set of CC3M and 30k samples from the MS-COCO’s validation split. For all models, we
406 sample the images at the resolution of 768 and resize them to 256 for calculating the metrics, using
407 the 25-steps PNDM (Liu et al., 2022) sampler following BK-SDM (Kim et al., 2023). We refer to
408 Appendix E for more details.
409

410 4.1 COMPARISON RESULTS

411
412 As APTP is the first pruning method specifically designed to prune a pretrained T2I model on a *target*
413 dataset, we compare its performance with SD V2.1, weight norm pruning (Li et al., 2017), and two
414 recently proposed static pruning baselines, namely Structural Pruning (SP) (Fang et al., 2023) and
415 BKSDM (Kim et al., 2023). Table 1 shows the results. We fine-tune APTP, SP and BKSDM for 30k
416 iterations after pruning and give Norm-pruning 50k fine-tuning iterations to ensure they all reach
417 their final performance level.

418 **CC3M:** Table 1a summarizes the results on CC3M. With a similar MACs budget and latency values,
419 APTP (0.85) significantly outperforms the Norm pruning (Li et al., 2017), SP (Fang et al., 2023),
420 and BKSDM (Kim et al., 2023) baselines with a significant margin in terms of FID, CLIP, and
421 CMMD scores. It also achieves 15% less latency while showing close performance scores to SD
422 V2.1. Notably, APTP (0.66) has approximately 23% less latency and 21% lower MACs budget than
423 the baselines, but it still outperforms them on all metrics. These results illustrate the advantages of
424 prompt-based compared to static pruning.

425 **MS-COCO:** We present the results for MS-COCO in Table 1b. APTP (0.78) reduces the latency of
426 SD by 22.5% while preserving its CLIP score and achieving a close CMMD score. Further, with
427 a similar latency, APTP (0.78) significantly outperforms the static pruning baselines with at least
428 3.71 FID (BKSDM), 2.34 CLIP (SP), and 0.042 CMMD (BKSDM) scores. Similar to the results on
429 CC3M, APTP (0.64) achieves approximately 19.3% less latency than the Norm pruning and SP while
430 outperforming them on all scores. In summary, our quantitative evaluations show the clear advantage
431 of prompt-based compared to static pruning for T2I models. We provide samples of APTP on the
validation sets of CC3M and MS-COCO in Fig. 3 and Appendix E.4.6.

Table 1: Results on CC3M and MS-COCO. We report performance metrics using samples generated at the resolution of 768 then downsampled to 256 (Kim et al., 2023). We measure models’ MACs/Latency with the input resolution of 768 on an A100 GPU. @30/50k shows fine-tuning iterations after pruning.

CC3M						MS-COCO					
Method	Complexity		Performance			Method	Complexity		Performance		
	MACs (@768)	Latency (↓) (Sec/Sample) (@768)	FID (↓)	CLIP (↑)	CMMD (↓)		MACs (@768)	Latency (↓) (Sec/Sample) (@768)	FID (↓)	CLIP (↑)	CMMD (↓)
Norm (Li et al., 2017) @50k	1185.3G	3.4	141.04	26.51	1.646	Norm (Li et al., 2017) @50k	1077.4G	3.1	47.35	28.51	1.136
SP (Fang et al., 2023) @30k	1192.1G	3.5	75.81	26.83	1.243	SP (Fang et al., 2023) @30k	1071.4G	3.3	53.09	28.98	0.926
BKSDM (Kim et al., 2023) @30k	1180.0G	3.3	87.27	26.56	1.679	BKSDM (Kim et al., 2023) @30k	1085.4G	3.1	26.31	28.89	0.611
APTP(0.66) @30k	916.3G	2.6	60.04	28.64	1.094	APTP(0.64) @30k	890.0G	2.5	39.12	29.98	0.867
APTP(0.85) @30k	1182.8G	3.4	36.77	30.84	0.675	APTP(0.78) @30k	1076.6G	3.1	22.60	31.32	0.569
SD 2.1	1384.2G	4.0	32.08	31.12	0.567	SD 2.1	1384.2G	4.0	15.47	31.33	0.500

(a)

(b)

Table 2: The most frequent words in prompts assigned to each expert of APTP-Base pruned on CC3M. The resource utilization of each expert is indicated in parentheses.

Expert 1 (0.72)	Expert 2 (0.73)	Expert 3 (0.75)	Expert 4 (0.76)
View - Sunset - City - Building - Sky	View - Boat - Sea	Artist - Actor	Actor - Dress - Portrait
Expert 5 (0.77)	Expert 6 (0.78)	Expert 7 (0.79)	Expert 8 (0.79)
Illustration - Portrait - Photo	Player - Ball - Game - Team	Background - Water - River - Tree	Biological Species - Dog - Cat
Expert 9 (0.79)	Expert 10 (0.80)	Expert 11 (0.81)	Expert 12 (0.81)
Illustration - Vector	People	Car - City - Road	Person - Player - Team - Couple
Expert 13 (0.86)	Expert 14 (0.90)	Expert 15 (0.95)	Expert 16 (0.98)
Room - House	Art - Artist - Digital	Food - Water	Person - Man - Woman - Text

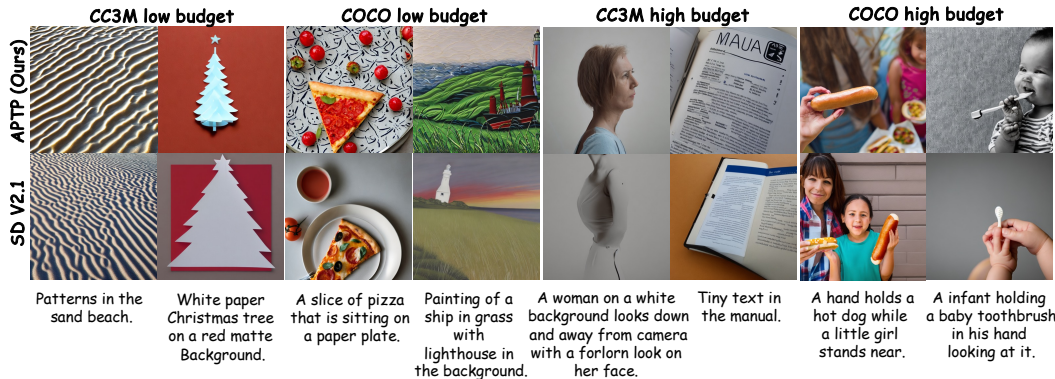


Figure 4: Comparison of samples generated by low and high budget experts of APTP-Base vs. SD V2.1 on CC3M and MS-COCO validation sets.

4.2 ANALYSIS OF THE PROMPT ROUTER

We analyze our prompt router’s behavior by examining the prompts it assigns to experts in the APTP-Base (0.85) model for the CC3M experiment. Table 2 displays the most frequent words in the prompts routed to each expert, along with the experts’ MACs budgets. Our prompt router effectively “specializes” experts by assigning distinct topics to experts with varying budgets. For instance, Expert 1 focuses on cityscapes, Expert 8 on animals, and Expert 13 on house interiors and exteriors. Notably, the prompt router assigns images of textual content and human beings to Expert 16, which has the highest budget. These categories have been empirically found to be challenging for SD 2.1 (Chen et al., 2024; Yang et al., 2024), and our prompt router can automatically discover and route them to higher-capacity experts. In contrast, paintings and illustrations are assigned to lower-budget experts, as they seem to be easier for the model to generate. We provide examples of high and low resource prompts for APTP-Base on both CC3M and COCO in Fig. 4.

4.3 ABLATION STUDY

We conduct two ablation experiments to study the impact of APTP’s components on its performance. First, we implement a naive baseline that uses parameterizations $\mathbf{v} = \text{sigmoid}((\eta_v + g_v)/\tau)$ and $\mathbf{u} = \text{sigmoid}((\eta_u + g_u)/\tau)$ (Eq. 9) to prune a single model. It directly trains two vectors (η_v, η_u) to do so (‘Uni-Arch Baseline’ in Table 3). Then, we start with a router trained only using the contrastive objective (Eq. 13) and add optimal transport and distillation incrementally to prune SD V2.1 into 8 experts with 80% MACs budget on MS-COCO (Lin et al., 2014). We fine-tune all pruned models with 10k iterations, and Table 3 presents the results. We observe that the contrastive training (Eq. 13) alone fails to improve results from pruning a single model to a mixture of experts. This is because although the contrastive objective makes the architecture codes diverse, it does not enforce the prompt router to distribute the prompts between architecture codes. Thus, it routes most of the input prompts to a single expert. As a result, all experts except one receive insufficient training samples and generate low-quality samples after fine-tuning, leading to the mixture showing worse metrics than the baseline. Employing optimal transport (Eq. 5) in the prompt router significantly improves FID (10.22), CLIP (1.17), and CMMD (0.18) scores of the mixture. In addition, distillation can further improve the architecture search process of the experts, resulting in a more performant mixture. In summary, these results validate the effectiveness of our design choices for APTP.

Table 3: Ablation results of APTP’s components on 30k samples from MS-COCO (Lin et al., 2014) validation set. We fine-tune all models for 10k iterations after pruning.

Method	MACs(@768)	Latency(@768)	FID (↓)	Clip Score (↑)	CMMD (↓)
Uni-Arch Baseline	1088.8G	3.1	46.56	29.11	0.91
Contrastive Router	1079.5G	3.1	48.78	28.90	0.92
+ Optimal Transport	1076.6G	3.1	38.56	30.07	0.74
+ Distillation (APT)	1076.6G	3.1	25.57	31.13	0.58

In our second ablation experiment, we explore the impact of the number of experts on APTP. We prune SD V2.1 to 80% MACs budget using APTP with 4, 8, and 12 experts on MS-COCO. Fig. 5 shows the results. Interestingly, the results demonstrate that the relationship between FID and CLIP scores with the number of experts is nonlinear, and the optimal number of experts is dataset-dependent. This observation illustrates that prompt-based pruning is more suitable than static pruning for T2I models.

5 CONCLUSION

In this paper, we develop Adaptive Prompt-Tailored Pruning (APT), the first prompt-based pruning method for text-to-image (T2I) diffusion models. APT takes a T2I model, pretrained on large-scale data, and prunes it using a *target* dataset, resembling the common practice that organizations fine-tune T2I models on their internal data before deployment. The core element of APT is a prompt router module that learns to decide the model capacity required to generate a sample for an input prompt, routing it to an architecture code given a desired compute budget. Each architecture code corresponds to a sub-network of the T2I model, specializing in generating images for the prompts that prompt router routes to it. APT trains the prompt router and architecture codes in an end-to-end manner, encouraging the prompt router to route similar prompts to similar architecture codes. Further, we utilize optimal transport in the prompt router of APT during pruning to diversify the architecture codes. Our experiments in which we prune Stable Diffusion (SD) V2.1 using CC3M and MS-COCO as *target* datasets demonstrate the benefit of prompt-based pruning compared to conventional static pruning methods for T2I models. Further, our analysis on APT’s prompt router reveals that it can automatically discover challenging prompt types for SD, like generating text, humans, and fingers, routing them to experts with high compute budgets.

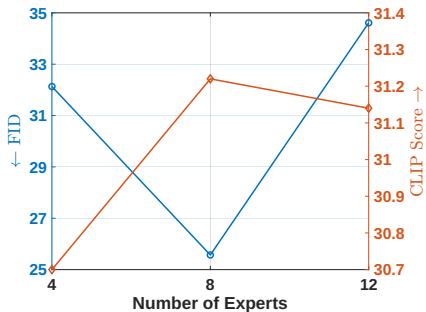


Figure 5: Ablation Results for the number of experts of APT on MS-COCO.

REFERENCES

- 540
541
542 Adobe FireFly. Firefly, 2023. URL [https://www.adobe.com/sensei/generative-ai/
543 firefly.html](https://www.adobe.com/sensei/generative-ai/firefly.html).
- 544 Shubham Agarwal, Subrata Mitra, Sarthak Chakraborty, Srikrishna Karanam, Koyel Mukherjee,
545 and Shiv Saini. Approximate caching for efficiently serving diffusion models. *arXiv preprint
546 arXiv:2312.04429*, 2023.
- 547
548 James Betker, Gabriel Goh, Li Jing, Tim Brooks, Jianfeng Wang, Linjie Li, Long Ouyang, Juntang
549 Zhuang, Joyce Lee, Yufei Guo, et al. Improving image generation with better captions. *Computer
550 Science*. <https://cdn.openai.com/papers/dall-e-3.pdf>, 2(3):8, 2023.
- 551 Han Cai, Chuang Gan, Tianzhe Wang, Zhekai Zhang, and Song Han. Once-for-all: Train one
552 network and specialize it for efficient deployment. In *International Conference on Learning
553 Representations*, 2020. URL <https://openreview.net/forum?id=HylxE1HKwS>.
- 554 Mathilde Caron, Ishan Misra, Julien Mairal, Priya Goyal, Piotr Bojanowski, and Armand Joulin.
555 Unsupervised learning of visual features by contrasting cluster assignments. *Advances in neural
556 information processing systems*, 33:9912–9924, 2020.
- 557
558 Thibault Castells, Hyoung-Kyu Song, Bo-Kyeong Kim, and Shinkook Choi. Ld-pruner: Efficient
559 pruning of latent diffusion models using task-agnostic insights. In *IEEE/CVF Conference on
560 Computer Vision and Pattern Recognition, CVPR 2024 - Workshops, Seattle, WA, USA, June
561 17-18, 2024*, pp. 821–830. IEEE, 2024. doi: 10.1109/CVPRW63382.2024.00087. URL [https:
562 //doi.org/10.1109/CVPRW63382.2024.00087](https://doi.org/10.1109/CVPRW63382.2024.00087).
- 563 Haoxing Chen, Zhuoer Xu, Zhangxuan Gu, Yaohui Li, Changhua Meng, Huijia Zhu, Weiqiang Wang,
564 et al. Diffute: Universal text editing diffusion model. *Advances in Neural Information Processing
565 Systems*, 36, 2024.
- 566
567 Hongrong Cheng, Miao Zhang, and Javen Qinfeng Shi. A survey on deep neural network pruning-
568 taxonomy, comparison, analysis, and recommendations. *arXiv preprint arXiv:2308.06767*, 2023.
- 569 Huanpeng Chu, Wei Wu, Chengjie Zang, and Kun Yuan. Qncd: Quantization noise correction for
570 diffusion models. *arXiv preprint arXiv:2403.19140*, 2024.
- 571
572 Marco Cuturi. Sinkhorn distances: Lightspeed computation of optimal transport. *Advances in neural
573 information processing systems*, 26, 2013.
- 574 Sara Elkerdawy, Mostafa Elhoushi, Hong Zhang, and Nilanjan Ray. Fire together wire together: A
575 dynamic pruning approach with self-supervised mask prediction. In *Proceedings of the IEEE/CVF
576 Conference on Computer Vision and Pattern Recognition*, pp. 12454–12463, 2022.
- 577
578 Gongfan Fang, Xinyin Ma, and Xinchao Wang. Structural pruning for diffusion models. In *Advances
579 in Neural Information Processing Systems*, 2023.
- 580 Rohit Gandikota, Joanna Materzynska, Tingrui Zhou, Antonio Torralba, and David Bau. Concept
581 sliders: Lora adaptors for precise control in diffusion models. *arXiv preprint arXiv:2311.12092*,
582 2023.
- 583
584 Emil Julius Gumbel. *Statistical theory of extreme values and some practical applications: a series of
585 lectures*, volume 33. US Government Printing Office, 1954.
- 586 Amirhossein Habibian, Amir Ghodrati, Noor Fathima, Guillaume Sautiere, Risheek Garrepalli, Fatih
587 Porikli, and Jens Petersen. Clockwork diffusion: Efficient generation with model-step distillation.
588 *arXiv preprint arXiv:2312.08128*, 2023.
- 589
590 Song Han, Jeff Pool, John Tran, and William Dally. Learning both weights and connections for
591 efficient neural network. *Advances in neural information processing systems*, 28, 2015.
- 592
593 Kaiming He, Xiangyu Zhang, Shaoqing Ren, and Jian Sun. Deep residual learning for image
recognition. In *Proceedings of the IEEE conference on computer vision and pattern recognition*,
pp. 770–778, 2016.

- 594 Yang He and Lingao Xiao. Structured pruning for deep convolutional neural networks: A survey.
595 *IEEE Transactions on Pattern Analysis and Machine Intelligence*, pp. 1–20, 2023. doi: 10.1109/
596 TPAMI.2023.3334614.
- 597 Yefei He, Luping Liu, Jing Liu, Weijia Wu, Hong Zhou, and Bohan Zhuang. Ptdq: Accurate post-
598 training quantization for diffusion models. *Advances in Neural Information Processing Systems*,
599 36, 2024.
- 601 Yihui He, Ji Lin, Zhijian Liu, Hanrui Wang, Li-Jia Li, and Song Han. Amc: Automl for model
602 compression and acceleration on mobile devices. In *Proceedings of the European conference on*
603 *computer vision (ECCV)*, pp. 784–800, 2018.
- 605 Amir Hertz, Ron Mokady, Jay Tenenbaum, Kfir Aberman, Yael Pritch, and Daniel Cohen-Or. Prompt-
606 to-prompt image editing with cross attention control. *arXiv preprint arXiv:2208.01626*, 2022.
- 607 Jack Hessel, Ari Holtzman, Maxwell Forbes, Ronan Le Bras, and Yejin Choi. Clipscore: A reference-
608 free evaluation metric for image captioning. *arXiv preprint arXiv:2104.08718*, 2021.
- 610 Martin Heusel, Hubert Ramsauer, Thomas Unterthiner, Bernhard Nessler, and Sepp Hochreiter. Gans
611 trained by a two time-scale update rule converge to a local nash equilibrium. *Advances in neural*
612 *information processing systems*, 30, 2017.
- 614 Geoffrey Hinton, Oriol Vinyals, and Jeff Dean. Distilling the knowledge in a neural network. *arXiv*
615 *preprint arXiv:1503.02531*, 2015.
- 616 Jonathan Ho and Tim Salimans. Classifier-free diffusion guidance. *CoRR*, abs/2207.12598, 2022.
617 doi: 10.48550/ARXIV.2207.12598. URL [https://doi.org/10.48550/arXiv.2207.](https://doi.org/10.48550/arXiv.2207.12598)
618 [12598](https://doi.org/10.48550/arXiv.2207.12598).
- 620 Jonathan Ho, Ajay Jain, and Pieter Abbeel. Denoising diffusion probabilistic models. *Advances in*
621 *neural information processing systems*, 33:6840–6851, 2020.
- 622 Lu Hou, Zhiqi Huang, Lifeng Shang, Xin Jiang, Xiao Chen, and Qun Liu. Dynabert: Dynamic
623 bert with adaptive width and depth. *Advances in Neural Information Processing Systems*, 33:
624 9782–9793, 2020.
- 626 Eric Jang, Shixiang Gu, and Ben Poole. Categorical reparameterization with gumbel-softmax. In
627 *International Conference on Learning Representations*, 2017. URL [https://openreview.](https://openreview.net/forum?id=rkE3y85ee)
628 [net/forum?id=rkE3y85ee](https://openreview.net/forum?id=rkE3y85ee).
- 630 Sadeep Jayasumana, Srikumar Ramalingam, Andreas Veit, Daniel Glasner, Ayan Chakrabarti, and
631 Sanjiv Kumar. Rethinking fid: Towards a better evaluation metric for image generation. *arXiv*
632 *preprint arXiv:2401.09603*, 2023.
- 633 Bo-Kyeong Kim, Hyoung-Kyu Song, Thibault Castells, and Shinkook Choi. On architectural
634 compression of text-to-image diffusion models. *arXiv preprint arXiv:2305.15798*, 2023.
- 635 Gwanghyun Kim, Taesung Kwon, and Jong Chul Ye. Diffusionclip: Text-guided diffusion models
636 for robust image manipulation. In *Proceedings of the IEEE/CVF Conference on Computer Vision*
637 *and Pattern Recognition*, pp. 2426–2435, 2022.
- 639 Yuval Kirstain, Adam Polyak, Uriel Singer, Shahbuland Matiana, Joe Penna, and Omer Levy.
640 Pick-a-pic: An open dataset of user preferences for text-to-image generation. In Alice Oh,
641 Tristan Naumann, Amir Globerson, Kate Saenko, Moritz Hardt, and Sergey Levine (eds.),
642 *Advances in Neural Information Processing Systems 36: Annual Conference on Neural In-*
643 *formation Processing Systems 2023, NeurIPS 2023, New Orleans, LA, USA, December 10 -*
644 *16, 2023*, 2023. URL [http://papers.nips.cc/paper_files/paper/2023/hash/](http://papers.nips.cc/paper_files/paper/2023/hash/73aacd8b3b05b4b503d58310b523553c-Abstract-Conference.html)
645 [73aacd8b3b05b4b503d58310b523553c-Abstract-Conference.html](http://papers.nips.cc/paper_files/paper/2023/hash/73aacd8b3b05b4b503d58310b523553c-Abstract-Conference.html).
- 646 Ashish Kumar, Daneul Kim, Jaesik Park, and Laxmidhar Behera. Pick-or-mix: Dynamic channel sam-
647 pling for convnets, 2024. URL <https://openreview.net/forum?id=Howb7fXB4V>.

- 648 Yunsung Lee, JinYoung Kim, Hyojun Go, Myeongho Jeong, Shinhyeok Oh, and Seungtaek Choi.
649 Multi-architecture multi-expert diffusion models. In *Proceedings of the AAAI Conference on*
650 *Artificial Intelligence*, volume 38, pp. 13427–13436, 2024.
- 651
- 652 Hao Li, Asim Kadav, Igor Durdanovic, Hanan Samet, and Hans Peter Graf. Pruning filters for
653 efficient convnets. In *International Conference on Learning Representations*, 2017. URL <https://openreview.net/forum?id=rJqFGTslg>.
- 654
- 655 Xiuyu Li, Yijiang Liu, Long Lian, Huanrui Yang, Zhen Dong, Daniel Kang, Shanghang Zhang,
656 and Kurt Keutzer. Q-diffusion: Quantizing diffusion models. In *Proceedings of the IEEE/CVF*
657 *International Conference on Computer Vision*, pp. 17535–17545, 2023.
- 658
- 659 Yanyu Li, Huan Wang, Qing Jin, Ju Hu, Pavlo Chemerys, Yun Fu, Yanzhi Wang, Sergey Tulyakov,
660 and Jian Ren. Snapfusion: Text-to-image diffusion model on mobile devices within two seconds.
661 *Advances in Neural Information Processing Systems*, 36, 2024.
- 662
- 663 Tao Lin, Sebastian U. Stich, Luis Barba, Daniil Dmitriev, and Martin Jaggi. Dynamic model
664 pruning with feedback. In *International Conference on Learning Representations*, 2020. URL
665 <https://openreview.net/forum?id=SJem8lSFwB>.
- 666
- 667 Tsung-Yi Lin, Michael Maire, Serge Belongie, James Hays, Pietro Perona, Deva Ramanan, Piotr
668 Dollár, and C Lawrence Zitnick. Microsoft coco: Common objects in context. In *Computer Vision–*
669 *ECCV 2014: 13th European Conference, Zurich, Switzerland, September 6-12, 2014, Proceedings,*
670 *Part V 13*, pp. 740–755. Springer, 2014.
- 671
- 672 Enshu Liu, Xuefei Ning, Zinan Lin, Huazhong Yang, and Yu Wang. Oms-dpm: Optimizing the
673 model schedule for diffusion probabilistic models. *arXiv preprint arXiv:2306.08860*, 2023a.
- 674
- 675 Enshu Liu, Xuefei Ning, Huazhong Yang, and Yu Wang. A unified sampling framework for solver
676 searching of diffusion probabilistic models. *arXiv preprint arXiv:2312.07243*, 2023b.
- 677
- 678 Hanxiao Liu, Karen Simonyan, and Yiming Yang. DARTS: Differentiable architecture search. In
679 *International Conference on Learning Representations*, 2019. URL <https://openreview.net/forum?id=S1eYHoC5FX>.
- 680
- 681 Luping Liu, Yi Ren, Zhijie Lin, and Zhou Zhao. Pseudo numerical methods for diffusion models
682 on manifolds. In *The Tenth International Conference on Learning Representations, ICLR 2022,*
683 *Virtual Event, April 25-29, 2022*. OpenReview.net, 2022. URL <https://openreview.net/forum?id=PlKWVd2yBkY>.
- 684
- 685 Xingchao Liu, Xiwen Zhang, Jianzhu Ma, Jian Peng, and Qiang Liu. InstafLOW: One step is enough
686 for high-quality diffusion-based text-to-image generation. In *The Twelfth International Conference*
687 *on Learning Representations, ICLR 2024, Vienna, Austria, May 7-11, 2024*. OpenReview.net,
688 2024a. URL <https://openreview.net/forum?id=1k4yZbbDqX>.
- 689
- 690 Xuewen Liu, Zhikai Li, Junrui Xiao, and Qingyi Gu. Enhanced distribution alignment for post-training
691 quantization of diffusion models. *arXiv preprint arXiv:2401.04585*, 2024b.
- 692
- 693 Ilya Loshchilov and Frank Hutter. Decoupled weight decay regularization. In *7th International*
694 *Conference on Learning Representations, ICLR 2019, New Orleans, LA, USA, May 6-9, 2019*.
695 OpenReview.net, 2019. URL <https://openreview.net/forum?id=Bkg6RiCqY7>.
- 696
- 697 Cheng Lu, Yuhao Zhou, Fan Bao, Jianfei Chen, Chongxuan Li, and Jun Zhu. DPM-solver++:
698 Fast solver for guided sampling of diffusion probabilistic models, 2023. URL <https://openreview.net/forum?id=4vGwQqviud5>.
- 699
- 700 Xinyin Ma, Gongfan Fang, and Xinchao Wang. Deepcache: Accelerating diffusion models for free.
701 *arXiv preprint arXiv:2312.00858*, 2023.
- 702
- 703 Chris J. Maddison, Andriy Mnih, and Yee Whye Teh. The concrete distribution: A continuous
704 relaxation of discrete random variables. In *International Conference on Learning Representations*,
705 2017. URL <https://openreview.net/forum?id=S1jE5L5gl>.

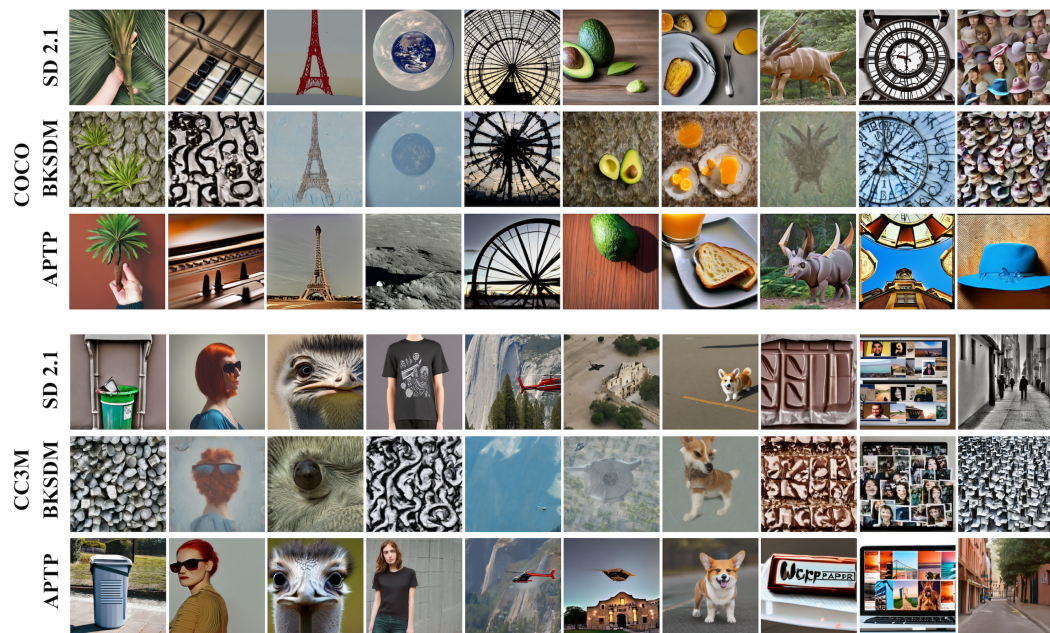
- 702 Chenlin Meng, Robin Rombach, Ruiqi Gao, Diederik Kingma, Stefano Ermon, Jonathan Ho, and Tim
703 Salimans. On distillation of guided diffusion models. In *Proceedings of the IEEE/CVF Conference*
704 *on Computer Vision and Pattern Recognition*, pp. 14297–14306, 2023.
- 705
706 Midjourney. Midjourney, 2023. URL <https://www.midjourney.com/home>.
- 707 Alex Nichol, Prafulla Dhariwal, Aditya Ramesh, Pranav Shyam, Pamela Mishkin, Bob McGrew,
708 Ilya Sutskever, and Mark Chen. Glide: Towards photorealistic image generation and editing with
709 text-guided diffusion models. *arXiv preprint arXiv:2112.10741*, 2021.
- 710
711 Alexander Quinn Nichol and Prafulla Dhariwal. Improved denoising diffusion probabilistic models.
712 In *International Conference on Machine Learning*, pp. 8162–8171. PMLR, 2021.
- 713 Zizheng Pan, Bohan Zhuang, De-An Huang, Weili Nie, Zhiding Yu, Chaowei Xiao, Jianfei Cai,
714 and Anima Anandkumar. T-stitch: Accelerating sampling in pre-trained diffusion models with
715 trajectory stitching. *arXiv preprint arXiv:2402.14167*, 2024.
- 716
717 Nilesh Prasad Pandey, Marios Fournarakis, Chirag Patel, and Markus Nagel. Softmax bias correction
718 for quantized generative models. In *Proceedings of the IEEE/CVF International Conference on*
719 *Computer Vision*, pp. 1453–1458, 2023.
- 720 Dustin Podell, Zion English, Kyle Lacey, Andreas Blattmann, Tim Dockhorn, Jonas Müller, Joe
721 Penna, and Robin Rombach. SDXL: Improving latent diffusion models for high-resolution image
722 synthesis. In *The Twelfth International Conference on Learning Representations*, 2024. URL
723 <https://openreview.net/forum?id=di52zR8xgf>.
- 724
725 Aditya Ramesh, Prafulla Dhariwal, Alex Nichol, Casey Chu, and Mark Chen. Hierarchical text-
726 conditional image generation with clip latents. *arXiv preprint arXiv:2204.06125*, 1(2):3, 2022.
- 727 Nils Reimers and Iryna Gurevych. Sentence-BERT: Sentence embeddings using Siamese BERT-
728 networks. In Kentaro Inui, Jing Jiang, Vincent Ng, and Xiaojun Wan (eds.), *Proceedings of the*
729 *2019 Conference on Empirical Methods in Natural Language Processing and the 9th International*
730 *Joint Conference on Natural Language Processing (EMNLP-IJCNLP)*, pp. 3982–3992, Hong Kong,
731 China, November 2019. Association for Computational Linguistics. doi: 10.18653/v1/D19-1410.
732 URL <https://aclanthology.org/D19-1410>.
- 733 Robin Rombach, Andreas Blattmann, Dominik Lorenz, Patrick Esser, and Björn Ommer. High-
734 resolution image synthesis with latent diffusion models. In *Proceedings of the IEEE/CVF confer-*
735 *ence on computer vision and pattern recognition*, pp. 10684–10695, 2022.
- 736
737 Olaf Ronneberger, Philipp Fischer, and Thomas Brox. U-net: Convolutional networks for biomedical
738 image segmentation. In *Medical Image Computing and Computer-Assisted Intervention–MICCAI*
739 *2015: 18th International Conference, Munich, Germany, October 5-9, 2015, Proceedings, Part III*
740 *18*, pp. 234–241. Springer, 2015.
- 741 Chitwan Saharia, William Chan, Saurabh Saxena, Lala Li, Jay Whang, Emily L Denton, Kamyar
742 Ghasemipour, Raphael Gontijo Lopes, Burcu Karagol Ayan, Tim Salimans, et al. Photorealistic
743 text-to-image diffusion models with deep language understanding. *Advances in neural information*
744 *processing systems*, 35:36479–36494, 2022.
- 745
746 Tim Salimans and Jonathan Ho. Progressive distillation for fast sampling of diffusion models. In
747 *International Conference on Learning Representations*, 2022. URL <https://openreview.net/forum?id=TIIdIXIpzhoI>.
- 748
749 Piyush Sharma, Nan Ding, Sebastian Goodman, and Radu Soricut. Conceptual captions: A cleaned,
750 hypernymed, image alt-text dataset for automatic image captioning. In *Proceedings of ACL*, 2018.
- 751 Junhyuk So, Jungwon Lee, Daehyun Ahn, Hyungjun Kim, and Eunhyeok Park. Temporal dynamic
752 quantization for diffusion models. *Advances in Neural Information Processing Systems*, 36, 2024.
- 753
754 Jascha Sohl-Dickstein, Eric Weiss, Niru Maheswaranathan, and Surya Ganguli. Deep unsupervised
755 learning using nonequilibrium thermodynamics. In *International conference on machine learning*,
pp. 2256–2265. PMLR, 2015.

- 756 Jiaming Song, Chenlin Meng, and Stefano Ermon. Denoising diffusion implicit models. In *International*
757 *Conference on Learning Representations*, 2021a. URL [https://openreview.net/](https://openreview.net/forum?id=St1giarCHLP)
758 [forum?id=St1giarCHLP](https://openreview.net/forum?id=St1giarCHLP).
- 759 Yang Song and Stefano Ermon. Generative modeling by estimating gradients of the data distribution.
760 *Advances in neural information processing systems*, 32, 2019.
- 761 Yang Song, Jascha Sohl-Dickstein, Diederik P Kingma, Abhishek Kumar, Stefano Ermon, and Ben
762 Poole. Score-based generative modeling through stochastic differential equations. In *International*
763 *Conference on Learning Representations*, 2021b. URL [https://openreview.net/](https://openreview.net/forum?id=PXTIG12RRHS)
764 [forum?id=PXTIG12RRHS](https://openreview.net/forum?id=PXTIG12RRHS).
- 765 Yuda Song, Zehao Sun, and Xuanwu Yin. Sdxs: Real-time one-step latent diffusion models with
766 image conditions. *arXiv preprint arXiv:2403.16627*, 2024.
- 767 Siao Tang, Xin Wang, Hong Chen, Chaoyu Guan, Zewen Wu, Yansong Tang, and Wenwu Zhu.
768 Post-training quantization with progressive calibration and activation relaxing for text-to-image
769 diffusion models. *arXiv preprint arXiv:2311.06322*, 2023.
- 770 Yehui Tang, Yunhe Wang, Yixing Xu, Yiping Deng, Chao Xu, Dacheng Tao, and Chang Xu. Manifold
771 regularized dynamic network pruning. In *Proceedings of the IEEE/CVF conference on computer*
772 *vision and pattern recognition*, pp. 5018–5028, 2021.
- 773 Ashish Vaswani, Noam Shazeer, Niki Parmar, Jakob Uszkoreit, Llion Jones, Aidan N Gomez, Łukasz
774 Kaiser, and Illia Polosukhin. Attention is all you need. *Advances in neural information processing*
775 *systems*, 30, 2017.
- 776 Daniel Watson, William Chan, Jonathan Ho, and Mohammad Norouzi. Learning fast samplers for dif-
777 fusion models by differentiating through sample quality. In *International Conference on Learning*
778 *Representations*, 2022a. URL [https://openreview.net/](https://openreview.net/forum?id=VFBjuF8HEp)
779 [forum?id=VFBjuF8HEp](https://openreview.net/forum?id=VFBjuF8HEp).
- 780 Daniel Watson, Jonathan Ho, Mohammad Norouzi, and William Chan. Learning to efficiently sample
781 from diffusion probabilistic models, 2022b. URL [https://openreview.net/](https://openreview.net/forum?id=LOz0xDpw4Y)
782 [forum?id=](https://openreview.net/forum?id=LOz0xDpw4Y)
783 [LOz0xDpw4Y](https://openreview.net/forum?id=LOz0xDpw4Y).
- 784 Colin White, Mahmoud Safari, Rhea Sukthanker, Binxin Ru, Thomas Elsken, Arber Zela, Debadeepta
785 Dey, and Frank Hutter. Neural architecture search: Insights from 1000 papers. *arXiv preprint*
786 *arXiv:2301.08727*, 2023.
- 787 Felix Wimbauer, Bichen Wu, Edgar Schoenfeld, Xiaoliang Dai, Ji Hou, Zijian He, Artsiom Sanakoyeu,
788 Peizhao Zhang, Sam Tsai, Jonas Kohler, et al. Cache me if you can: Accelerating diffusion models
789 through block caching. *arXiv preprint arXiv:2312.03209*, 2023.
- 790 Yilun Xu, Mingyang Deng, Xiang Cheng, Yonglong Tian, Ziming Liu, and Tommi Jaakkola. Restart
791 sampling for improving generative processes. *arXiv preprint arXiv:2306.14878*, 2023.
- 792 Zeyue Xue, Guanglu Song, Qiushan Guo, Boxiao Liu, Zhuofan Zong, Yu Liu, and Ping Luo.
793 RAPHAEL: text-to-image generation via large mixture of diffusion paths. In Alice Oh, Tris-
794 tan Naumann, Amir Globerson, Kate Saenko, Moritz Hardt, and Sergey Levine (eds.), *Ad-*
795 *vances in Neural Information Processing Systems 36: Annual Conference on Neural Infor-*
796 *mation Processing Systems 2023, NeurIPS 2023, New Orleans, LA, USA, December 10 -*
797 *16, 2023*, 2023. URL [http://papers.nips.cc/](http://papers.nips.cc/paper_files/paper/2023/hash/821655c7dc4836838cd8524d07f9d6fd-Abstract-Conference.html)
798 [paper/2023/hash/](http://papers.nips.cc/paper_files/paper/2023/hash/821655c7dc4836838cd8524d07f9d6fd-Abstract-Conference.html)
799 [821655c7dc4836838cd8524d07f9d6fd-Abstract-Conference.html](http://papers.nips.cc/paper_files/paper/2023/hash/821655c7dc4836838cd8524d07f9d6fd-Abstract-Conference.html).
- 800 Xingyi Yang, Daquan Zhou, Jiashi Feng, and Xinchao Wang. Diffusion probabilistic model made
801 slim. In *Proceedings of the IEEE/CVF Conference on Computer Vision and Pattern Recognition*,
802 pp. 22552–22562, 2023a.
- 803 Yuewei Yang, Xiaoliang Dai, Jialiang Wang, Peizhao Zhang, and Hongbo Zhang. Efficient quantiza-
804 tion strategies for latent diffusion models. *arXiv preprint arXiv:2312.05431*, 2023b.
- 805 Yukang Yang, Dongnan Gui, Yuhui Yuan, Weicong Liang, Haisong Ding, Han Hu, and Kai Chen.
806 Glyphcontrol: Glyph conditional control for visual text generation. *Advances in Neural Information*
807 *Processing Systems*, 36, 2024.
- 808
809

- 810 Lewei Yao, Renjie Pi, Hang Xu, Wei Zhang, Zhenguo Li, and Tong Zhang. Joint-detnas: Upgrade your
811 detector with nas, pruning and dynamic distillation. In *Proceedings of the IEEE/CVF conference*
812 *on computer vision and pattern recognition*, pp. 10175–10184, 2021.
- 813
- 814 Asano YM., Rupprecht C., and Vedaldi A. Self-labelling via simultaneous clustering and rep-
815 resentation learning. In *International Conference on Learning Representations*, 2020. URL
816 <https://openreview.net/forum?id=Hyx-jyBFPr>.
- 817 Jiahui Yu, Yuanzhong Xu, Jing Yu Koh, Thang Luong, Gunjan Baid, Zirui Wang, Vijay Vasudevan,
818 Alexander Ku, Yinfei Yang, Burcu Karagol Ayan, Ben Hutchinson, Wei Han, Zarana Parekh, Xin
819 Li, Han Zhang, Jason Baldridge, and Yonghui Wu. Scaling autoregressive models for content-rich
820 text-to-image generation. *Trans. Mach. Learn. Res.*, 2022, 2022. URL <https://openreview.net/forum?id=AFDcYJKhND>.
- 821
- 822 Huijie Zhang, Yifu Lu, Ismail Alkhouri, Saiprasad Ravishankar, Dogyoon Song, and Qing Qu.
823 Improving efficiency of diffusion models via multi-stage framework and tailored multi-decoder
824 architectures. *arXiv preprint arXiv:2312.09181*, 2023a.
- 825
- 826 Lvmin Zhang, Anyi Rao, and Maneesh Agrawala. Adding conditional control to text-to-image
827 diffusion models. In *Proceedings of the IEEE/CVF International Conference on Computer Vision*,
828 pp. 3836–3847, 2023b.
- 829
- 830 Qinsheng Zhang, Molei Tao, and Yongxin Chen. gDDIM: Generalized denoising diffusion implicit
831 models. In *The Eleventh International Conference on Learning Representations*, 2023c. URL
832 <https://openreview.net/forum?id=1hKE9qjvz->.
- 833
- 834 Yang Zhao, Yanwu Xu, Zhisheng Xiao, and Tingbo Hou. Mobilediffusion: Subsecond text-to-image
generation on mobile devices. *arXiv preprint arXiv:2311.16567*, 2023.
- 835
- 836 Barret Zoph and Quoc Le. Neural architecture search with reinforcement learning. In *International*
837 *Conference on Learning Representations*, 2017. URL <https://openreview.net/forum?id=r1Ue8Hcxg>.
- 838
- 839
- 840
- 841
- 842
- 843
- 844
- 845
- 846
- 847
- 848
- 849
- 850
- 851
- 852
- 853
- 854
- 855
- 856
- 857
- 858
- 859
- 860
- 861
- 862
- 863



882 Figure 6: APTP generalizes to various styles, even if they are not present in the target dataset.



905 Figure 7: A visual comparison of randomly sampled generated images from Stable Diffusion 2.1,
906 BKSDM (the best baseline), and APTP. The top section displays models trained on the COCO dataset,
907 while the bottom section showcases samples from models trained on CC3M. Overall, APTP produces
908 higher-quality images compared to the baseline.
909

911 A MORE VISUAL RESULTS

912 We provide samples from APTP pruned models on various styles in Fig. 6. APTP preserves the
913 original model’s versatility and generalizes well to out-of-distribution prompts.

914 We provide samples comparing APTP to the best baseline, namely BKSDM Kim et al. (2023)), on
915 different prompts from the PartiPrompts Yu et al. (2022) datasets in Fig. 7. APTP produces better
916 images compared to the baseline.
917

B RELATED WORK

Efficient Diffusion Models: Methods for accelerating and improving the efficiency of diffusion models fall into two categories. The first group focuses on reducing the complexity or the number of sampling steps of diffusion models. They use techniques like distillation Habibian et al. (2023); Meng et al. (2023); Salimans & Ho (2022); Song et al. (2024); Liu et al. (2024a), learning optimal denoising time-steps Watson et al. (2022b;a), designing improved noise schedules Nichol & Dhariwal (2021); Song et al. (2021a); Zhang et al. (2023c), caching intermediate computations Ma et al. (2023); Agarwal et al. (2023); Wimbauer et al. (2023), and proposing faster solvers Lu et al. (2023); Xu et al. (2023); Liu et al. (2023b). The second group is aimed at improving the architectural efficiency of diffusion models, which is the main focus of our paper. **Multi-expert** Lee et al. (2024); Zhang et al. (2023a); Liu et al. (2023a); Pan et al. (2024); Xue et al. (2023) methods employ multiple expert models each responsible for a separate part of the denoising process of diffusion models. These methods either design expert model architectures Lee et al. (2024); Zhang et al. (2023a); Xue et al. (2023), train several models with varying capacities from scratch Liu et al. (2023a), or utilize existing pretrained experts Liu et al. (2023a); Pan et al. (2024) with different capacities. However, pretrained experts are not necessarily available, and training several models from scratch, as required by multi-expert methods, is prohibitively expensive in practice. **Architecture Design** approaches Zhao et al. (2023); Yang et al. (2023a); Kim et al. (2023) redesign the architecture of diffusion models to enhance efficiency. MobileDiffusion Zhao et al. (2023) modifies the U-Net Ronneberger et al. (2015) architecture of Stable Diffusion (SD) based on empirical heuristics derived from the model’s performance on the MS-COCO Lin et al. (2014) dataset. BK-SDM Kim et al. (2023) removes some blocks from the U-Net model of SD and applies knowledge distillation from the original SD model to the pruned model. Spectral Diffusion Yang et al. (2023a) introduces a wavelet gating operation and performs frequency domain distillation from a pretrained teacher model into a small student model. Yet, generalization of the heuristics and design choices in the architecture design methods to other tasks and compute budgets is non-trivial. **Quantization** methods So et al. (2024); He et al. (2024); Pandey et al. (2023); Yang et al. (2023b); Liu et al. (2024b); Tang et al. (2023); Chu et al. (2024); Li et al. (2023) reduce the precision of model weights and activations during the forward pass to accelerate the sampling process. Different from these methods, SnapFusion Li et al. (2024) searches for an efficient architecture for T2I models. However, evaluating each action in the search process consumes about 2.5 A100 GPU hours, rendering it impractical for resource-constrained scenarios. Finally, SPDM Fang et al. (2023) estimates the importance of different weights in the model using Taylor expansion and removes the low-scored architectures. Despite their promising results, all these methods are ‘static’ in that they obtain an efficient model and utilize it for all inputs. This is suboptimal for T2I models as input prompts may vary in complexity, demanding different model capacity levels.

Pruning and Neural Architecture Search (NAS): Our paper also intersects with model pruning Cheng et al. (2023) and NAS Zoph & Le (2017); Liu et al. (2019); Cai et al. (2020); Yao et al. (2021); Hou et al. (2020); White et al. (2023) methods. These methods prune pretrained models and search for suitable architectures given a specific task and computational budget. Existing pruning techniques can be categorized into Static and Dynamic methods. Static pruning approaches He et al. (2018); Li et al. (2017); Han et al. (2015); Castells et al. (2024) prune a pretrained model and use the pruned model for all inputs. Conversely, dynamic pruning methods Elkerdawy et al. (2022); Kumar et al. (2024); Lin et al. (2020); Tang et al. (2021) employ a separate sub-network of the model for each input. Although static and dynamic pruning methods have been successful for image classification, they are not suitable to be directly applied to T2I models. Static pruning methods neglect prompt complexity and employ the same model for all prompts while dynamic pruning ideas cannot utilize batch-parallelism in GPUs. We refer to recent surveys White et al. (2023); He & Xiao (2023); Cheng et al. (2023) for a comprehensive review of pruning and NAS methods.

Our method distinguishes itself from existing approaches by introducing a prompt-based pruning technique for T2I models. This work marks the first instance where computational resources are allocated to prompts based on their individual complexities while ensuring optimal utilization and batch-parallelizability.

C OVERVIEW OF DIFFUSION MODELS

Given a random variable $\mathbf{x}_0 \sim \mathcal{P}$, the goal of diffusion models Sohl-Dickstein et al. (2015); Ho et al. (2020) is to model the underlying distribution \mathcal{P} using a training set $\mathcal{D} = \{x_0\}$ of samples. To do so, first, diffusion models define a forward process parameterized by t in which they gradually perturb each sample x_0 with Gaussian noise with the variance schedule of β_t :

$$q(x_t|x_{t-1}) = \mathcal{N}(x_t; \sqrt{1 - \beta_t}x_{t-1}, \beta_t I) \quad (16)$$

where $t \in [1, T]$. Thus, $q(x_t|x_0)$ has a Gaussian form:

$$q(x_t|x_0) = \mathcal{N}(x_t; \sqrt{\bar{\alpha}_t}x_0, (1 - \bar{\alpha}_t)I) \quad (17)$$

where $\alpha_t = 1 - \beta_t$ and $\bar{\alpha}_t = \prod_{i=1}^t \alpha_i$. The noise schedule β_t is usually selected Ho et al. (2020) such that $q(x_T) \rightarrow \mathcal{N}(0, I)$. Assuming β_t is small, diffusion models approximate the denoising distribution $q(x_{t-1}|x_t)$ by a parameterized Gaussian distribution $p_\theta(x_{t-1}|x_t) = \mathcal{N}(x_{t-1}; \frac{1}{\sqrt{\alpha_t}}(x_t - \frac{\beta_t}{\sqrt{1-\alpha_t}}\epsilon_\theta(x_t, t)), \sigma_t^2 I)$, and σ_t^2 is often set to β_t . Diffusion models implement $\epsilon_\theta(\cdot)$ with a neural network called the denoising model and train it with the variational evidence lower bound (ELBO) objective Ho et al. (2020):

$$\mathcal{L}_{\text{DDPM}}(\theta) = \mathbb{E}_{\substack{t \sim [1, T] \\ \epsilon \sim \mathcal{N}(0, I) \\ x_t \sim q(x_t|x_0)}} \|\epsilon(x_t, t; \theta) - \epsilon\|^2 \quad (18)$$

Similarly, T2I diffusion models train a denoising model using pairs of image and text prompts $(x_0, p) \sim \mathcal{P}$ to model the distribution $\mathcal{P}(\mathbf{x}_0|\mathbf{p})$ of images given an input text prompt:

$$\mathcal{L}_{\text{DDPM}}(\theta) = \mathbb{E}_{\substack{(x_0, p) \sim \mathcal{P} \\ t \sim [1, T] \\ \epsilon \sim \mathcal{N}(0, I) \\ x_t \sim q(x_t|x_0)}} \|\epsilon(x_t, p, t; \theta) - \epsilon\|^2 \quad (19)$$

T2I Diffusion models generate a new sample by sampling an initial noise from $x_T \sim p(x_T) = \mathcal{N}(0, I)$ and iteratively denoising it using the denoising model by sampling from $p_\theta(x_{t-1}|x_t, p)$. Thus, the sampling process requires T sequential forward calculation of the denoising model, making it a slow and costly process.

D MORE DETAILS OF APTP

In this section we provide more details of the architecture predictor, the prompt router module, and our pruning method.

D.1 ARCHITECTURE PREDICTOR

$f_{\text{AP}}(\cdot)$ in Eq. 4 is the architecture predictor. The architecture predictor changes the dimensionality of z to the dimensionality of e and codes a , which is the number of prunable width and depth units in the T2I model. We implement the f_{AP} function with a single feed-forward layer. Our prompt encoder, Sentence Transformer Reimers & Gurevych (2019), has an output dimension of **768**. The total number of prunable units in SD 2.1 is **1620**, so the architecture predictor has an input dimension of **768** and an output dimension of **1620** in all of our experiments.

D.2 ROUTER MODULE DEFINITION

During the pruning process, we use the assignment matrix Q^* calculated by optimal transport (Eq. 7) to route the architecture embeddings e to the architecture codes a . Thus, during the pruning process, the definition of function f_{R} is as follows:

1026
1027
1028
1029
1030
1031
1032
1033
1034
1035
1036
1037
1038
1039
1040
1041
1042
1043
1044
1045
1046
1047
1048
1049
1050
1051
1052
1053
1054
1055
1056
1057
1058
1059
1060
1061
1062
1063
1064
1065
1066
1067
1068
1069
1070
1071
1072
1073
1074
1075
1076
1077
1078
1079

$$I = \operatorname{argmax}(BQ^*, \dim = 0) \quad (20)$$

$$f_{\mathcal{R}}(e, \mathcal{A}, Q^*) = A[:, I] \quad (21)$$

where e represents the architecture embeddings in a pruning batch, \mathcal{A} is the set of architecture codes, Q^* is the calculated optimal assignment matrix, and A is the matrix of architecture codes.

At test time, the router function routes an input architecture embedding e to the most similar trained architecture code:

$$f_{\mathcal{R}}(e, \mathcal{A}) = \operatorname{argmax}_{a \in \mathcal{A}} \frac{e^T a}{\|e\| \|a\|} \quad (22)$$

D.3 PRUNING DEPTH

We apply the vectors $\mathbf{u}^{(i)} = [\mathbf{u}_j^{(i)}]_{j=1}^M$ (Eq. 9) to prune the model’s depth with M being the total number of layers we prune. As the U-Net Ronneberger et al. (2015) architecture of T2I models has skip connections, we prune the depth layers in the encoder and decoder sides separately.

Pruning Depth in Encoder. We prune the j -th depth layer f_j in the encoder by applying the vector $u_j^{(i)}$ with the following formulation:

$$\widehat{\mathcal{F}}_j = \mathbf{u}_j^{(i)} f_j(\mathcal{F}_{j-1}) + (1 - \mathbf{u}_j^{(i)}) \mathcal{F}_{j-1} \quad (23)$$

where \mathcal{F}_{j-1} is the feature maps of the previous layer. When $u_j^{(i)}$ is close to one/zero, the j -th layer will be kept/pruned.

Pruning Depth in Decoder. In the decoder, the input of each layer is a concatenation of feature maps of the previous layer and feature maps of its corresponding encoder layer from the skip connection $\mathcal{F}_{j,skip}$. Thus, we prune the j -th depth layer f_j in the decoder as:

$$\widehat{\mathcal{F}}_j = \mathbf{u}_j^{(i)} f_j(\mathcal{F}_{j-1} || \mathcal{F}_{j,skip}) + (1 - \mathbf{u}_j^{(i)}) \mathcal{F}_{j-1} \quad (24)$$

D.4 DISTILLATION OBJECTIVE

Assuming $B^{(i)}$ samples get routed to the architecture code $a^{(i)}$ in a training batch ($\sum_i B^{(i)} = B$), we train the prompt router and the architecture codes using the following objective:

$$\begin{aligned} \min_{\eta, \mathcal{A}} \mathcal{L} = & \left[\frac{1}{N} \sum_{i=1}^N \left[\frac{1}{B^{(i)}} \sum_{j=1}^{B^{(i)}} [\mathcal{L}_{\text{DDPM}}(x_j^{(i)}, p_j^{(i)}; a^{(i)}) + \lambda_{\text{distill}} \mathcal{L}_{\text{distill}}(x_j^{(i)}, p_j^{(i)}; a^{(i)})] \right] \right] \\ & + \lambda_{\text{res}} \mathcal{R}(\widehat{T}(\mathcal{A}), T_d) + \lambda_{\text{cont}} \mathcal{L}_{\text{cont}}(\eta) \end{aligned} \quad (25)$$

$\mathcal{L}_{\text{DDPM}}(x_j^{(i)}, p_j^{(i)}; a^{(i)})$ denotes the denoising objective for the sample $(x_j^{(i)}, p_j^{(i)})$ routed to the sub-network chosen by the architecture code $a^{(i)}$ (Eq. 19). $\mathcal{R}(\widehat{T}(\mathcal{A}), T_d)$ regularizes the weighted average of the MACs used by architecture codes ($\widehat{T}(\mathcal{A}) = \sum_i \frac{B^{(i)}}{B} \widehat{T}(a^{(i)})$) to be close to T_d . We define

$$\mathcal{R}(x, y) = \log(\max(x, y) / \min(x, y)) \quad (26)$$

as it can keep the resource usage close to the target value. $\mathcal{L}_{\text{cont}}$, given by Eq. 13, is the contrastive loss that guides the architecture predictor to map prompt representations to the regions of the space of the architecture embeddings such that their corresponding architecture vectors maintain the similarity between the prompts. Finally, $\mathcal{L}_{\text{distill}}$ is the distillation objective Hinton et al. (2015), regularizing the pruned model to have similar outputs to the original one. We do distillation at two levels, output level and block level. The output level distillation objective is:

$$\mathcal{L}_{\text{output-distill}}(x_j^{(i)}, p_j^{(i)}; a^{(i)}) = \mathbb{E}_{\substack{t \sim [1, T] \\ \epsilon \sim \mathcal{N}(0, I) \\ x_{j,t}^{(i)} \sim q(x_t | x_j^{(i)})}} [\|\epsilon_{\text{Teacher}}(x_{j,t}^{(i)}, p_j^{(i)}, t; \theta) - \epsilon_{\text{Sub-Net}}(x_{j,t}^{(i)}, p_j^{(i)}, t; \theta, a^{(i)})\|^2] \quad (27)$$

Here, $\epsilon_{\text{Teacher}}(x_{j,t}^{(i)}, p_j^{(i)}, t; \theta)$ denotes the original model’s output and $\epsilon_{\text{Sub-Net}}(x_{j,t}^{(i)}, p_j^{(i)}, t; \theta, a^{(i)})$ denotes the output of the sub-network chosen by the architecture code $a^{(i)}$. The way we prune the U-Net preserves the output shape of each block. Doing so enables us to do distillation at block level as well and regularize the sub-network to match the output of the original model at each block. The block-level distillation objective is:

$$\mathcal{L}_{\text{block-distill}}(x_j^{(i)}, p_j^{(i)}; a^{(i)}) = \mathbb{E}_{\substack{t \sim [1, T] \\ \epsilon \sim \mathcal{N}(0, I) \\ x_{j,t}^{(i)} \sim q(x_t | x_j^{(i)})}} [\sum_b \|\epsilon_{\text{Teacher}}^b(x_{j,t}^{(i)}, p_j^{(i)}, t; \theta) - \epsilon_{\text{Sub-Net}}^b(x_{j,t}^{(i)}, p_j^{(i)}, t; \theta, a^{(i)})\|^2] \quad (28)$$

Here, $\epsilon_{\text{Teacher}}^b$ and $\epsilon_{\text{Sub-Net}}^b$ denote the outputs of block b of the original model and the chosen sub-network of it, respectively. The total distillation loss $\mathcal{L}_{\text{distill}}$ is simply the sum of the output-level loss and the block-level distillation loss:

$$\mathcal{L}_{\text{distill}} = \mathcal{L}_{\text{output-distill}} + \mathcal{L}_{\text{block-distill}} \quad (29)$$

D.5 FINE-TUNING

The finetuning loss is a weighted average of the original DDPM objective (Eq. 19) and the distillation loss term (Eq. 29):

$$\mathcal{L}_{\text{finetuning}} = \alpha_{\text{DDPM}} \mathcal{L}_{\text{DDPM}} + \alpha_{\text{distill}} \mathcal{L}_{\text{distill}} \quad (30)$$

E EXPERIMENTS

E.1 MODELS AND DATASETS

We use two datasets as our *target* datasets: Conceptual Captions 3M (CC3M) Sharma et al. (2018) and MS-COCO Captions 2014 Lin et al. (2014) with approximately 2.5M and 400K image-caption pairs, respectively. We apply APTP to the Stable Diffusion 2.1 (SD 2.1) Rombach et al. (2022) model. On CC3M, we prune SD2.1 with two settings: Base (0.85 budget, 16 experts) and Small (0.66 budget, 8 experts). Similarly, for COCO, we have two settings: Base (0.78 budget, 8 experts) and Small (0.64 budget, 8 experts). We use a pruned SD 2.1 using weight norm pruning Li et al. (2017) as a baseline for our main experiments.

E.2 EXPERIMENTAL SETTINGS

We train at a fixed resolution of 256×256 across all settings. During pruning, we first train the architecture predictor for 500 iterations as a warm-up phase. During this warm-up phase, we directly use its predicted architectures for pruning. Then, we start architecture codes and train the architecture predictor jointly with the codes for an additional 2500 iterations. We use the AdamW Loshchilov & Hutter (2019) optimizer and a constant learning rate of 0.0002 for both modules, with a 100-iteration linear warm-up. The effective pruning batch size is 1024, achieved by training on 16 NVIDIA A100 GPUs with a local batch size of 64. The temperature of the Gumbel-Sigmoid reparametrization (Eq. 9) is set to $\gamma = 0.4$. We set the regularization strength of the optimal transport objective (Eq. 5) to $\epsilon = 0.05$. We use 3 iterations of the Sinkhorn-Knopp algorithm Cuturi (2013) to solve the optimal transport problem Caron et al. (2020). We set the contrastive loss temperature τ to 0.03. The total pruning loss is the weighted average of DDPM loss, distillation loss, resource loss, and contrastive loss (see Eq. 15) with weights $\lambda_{\text{distill}} = 0.2$, $\lambda_{\text{res}} = 2.0$, and $\lambda_{\text{cont}} = 100.0$. After the pruning phase,

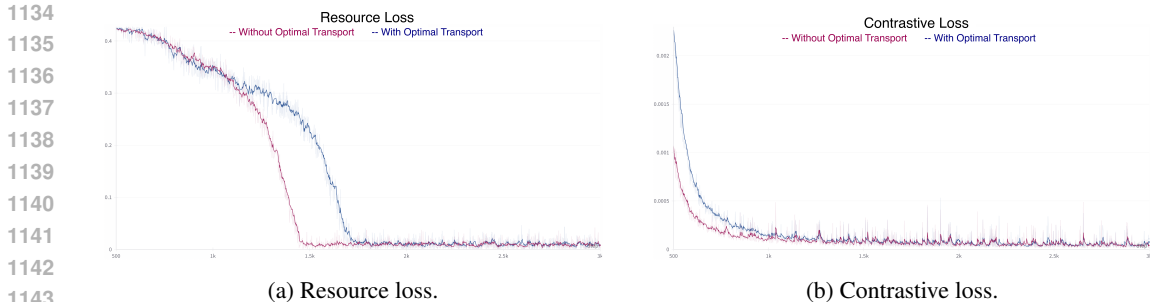


Figure 8: Resource and Contrastive loss observed when applying APTP-Base with a MAC budget of 0.77 to prune Stable Diffusion 2.1 using the COCO dataset. The comparison is made between two settings: with and without optimal transport. APTP both adheres to the target MAC budget and finds architecture vectors that maintain the similarity between the prompts.

we fine-tune the experts with the prompts assigned to them for 30,000 iterations using the AdamW optimizer, a fixed learning rate of 0.00001, and a batch size of 128. Upon experiments, we observed that higher weights of the DDPM loss result in unstable fine-tuning and slow convergence. As a result, we set the DDPM loss weight in the fine-tuning loss (Eq. 30) α_{DDPM} to 0.0001. We set $\alpha_{distill} = 1.0$. For sample generation, we use the classifier-free guidance Ho & Salimans (2022) technique with the scale of 7.5 and 25 steps of the PNDM sampler Liu et al. (2022).

E.3 EVALUATION

For quantitative evaluation of models pruned on CC3M, we use its validation dataset of approximately 14k samples. For COCO, we sample 30k captions of unique images from its 2014 validation dataset. We report Fréchet inception distance (FID) Heusel et al. (2017), CLIP score Hessel et al. (2021), and Maximum Mean Discrepancy with CLIP Embeddings (CMMD) Jayasumana et al. (2023) for APTP, the baselines, and SD 2.1 itself.

E.4 RESULTS

E.4.1 TRAINING LOSS

Introduced in section 3.3.1, the resource loss regularizes the weighted average of the MACs used by architecture codes ($\hat{T}(\mathcal{A}) = \sum_i \frac{B^{(i)}}{B} [\hat{T}(a^{(i)})]$) to be close to T_d . We define resource loss as:

$$\mathcal{R}(x, y) = \log(\max(x, y) / \min(x, y)) \tag{31}$$

Fig. 8a illustrates the resource loss when applying APTP-Base to prune Stable Diffusion 2.1 using the COCO dataset as the target. This is shown under two conditions: with and without optimal transport following the initial warm-up phase (refer to E for details). APTP effectively regularizes the model so average MACs of the architecture codes is very close to the target budget. Fig. 8b presents the contrastive loss (Eq. 13) under the same conditions. APTP maps the prompt embeddings to regions of architecture embeddings such that their corresponding architectures maintain the similarity between prompts.

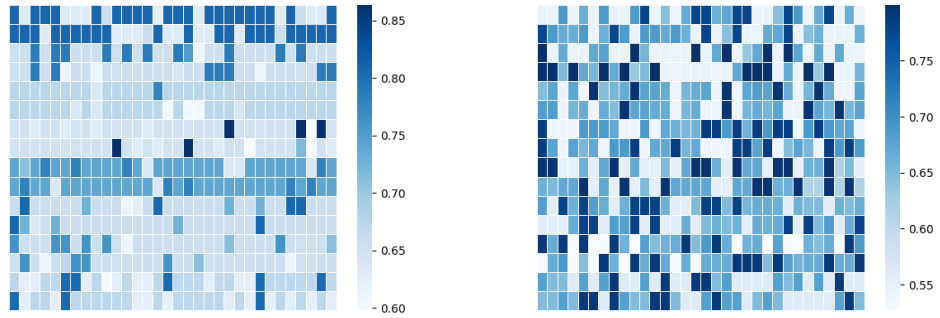
E.4.2 VISUALIZATION OF THE IMPACT OF OPTIMAL TRANSPORT

Fig. 9 displays the assignment of prompts to experts with and without optimal transport. By adding optimal transport, the assignment becomes more diverse, ensuring all experts get enough samples. This results in a significant improvement of performance metrics (See Table 3). Fig. 10 shows the distribution of the number of training CC3M samples mapped to each expert of APTP-Base.

E.4.3 ANALYSIS OF PROMPT ROUTER ON COCO

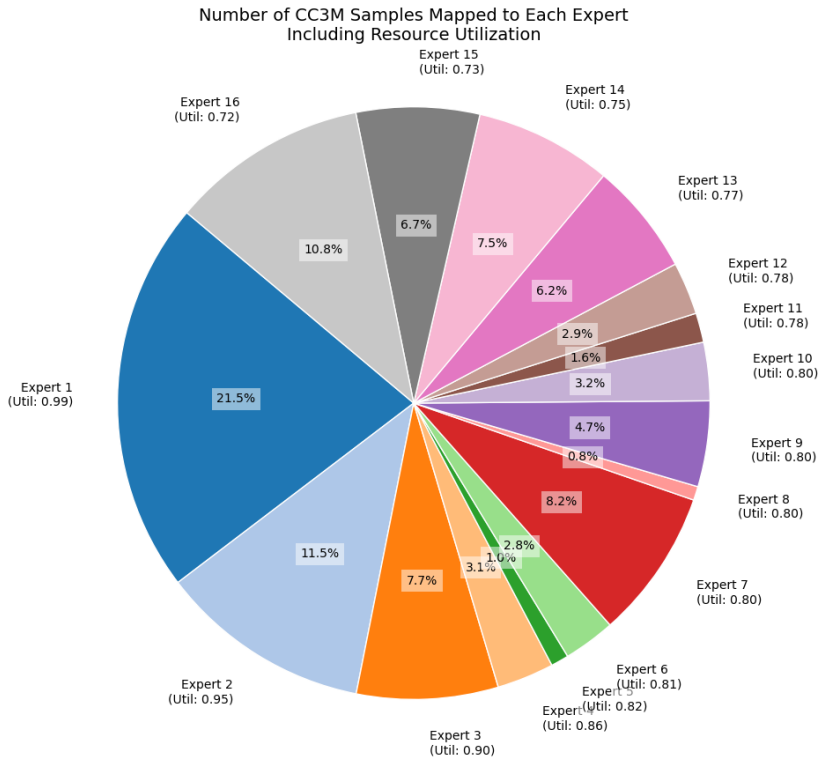
Table 4 demonstrates the most frequent words in the prompts assigned to each expert of APTP-Base pruned on COCO, revealing distinct topics and effective specialization. For example, Expert 1

1188
1189
1190
1191
1192
1193
1194
1195
1196
1197
1198
1199
1200
1201
1202
1203



1204 Figure 9: Comparison of sample assignments in a batch to experts with and without optimal transport.
1205 The incorporation of optimal transport results in a more diverse assignment pattern. In the figure,
1206 each square represents a prompt within the batch, and the color signifies the budget level of the expert
1207 assigned to the prompt. Higher-resource experts are indicated by darker blue.
1208
1209
1210
1211

1212
1213
1214
1215
1216
1217
1218
1219
1220
1221
1222
1223
1224
1225
1226
1227
1228
1229
1230
1231
1232
1233
1234
1235
1236
1237
1238



1239 Figure 10: Distribution of CC3M Samples Mapped to Each Expert of APTP-Base, Including Resource
1240 Utilization Ratios
1241

specializes in indoor scenes, Expert 5 in wildlife, and Expert 6 in urban scenes. Expert 8 which has the highest resource utilization, focuses on images of human beings and hands, an observation consistent with our prompt analysis on CC3M (Table 2). Hands are another category that have been found to be challenging for SD 2.1 Gandikota et al. (2023).

Table 4: The most frequent words in prompts assigned to each expert of APTP-Base pruned on COCO. The resource utilization of each expert is indicated in parentheses.

Expert 1 (0.65, Indoor Scenes and Dining)	Expert 2 (0.77, Food and Small Groups)
table - plate - kitchen - sitting	food - pizza - sandwich
Expert 3 (0.78, People and Objects)	Expert 4 (0.79, Sports and Activities)
skateboard - surfboard - laptop - tie - phone	tennis - baseball - racquet - skateboard - skis
Expert 5 (0.79, Wildlife and Nature)	Expert 6 (0.80, Urban Scenes and Transportation)
giraffe - herd - sheep - zebra - elephants	street - train - bus - park - building
Expert 7 (0.81, Outdoor Activities and Nature)	Expert 8 (0.83, Domestic Life and Pets)
beach - ocean - surfboard - kite - wave	man - woman - girl - hand - bed - cat

E.4.4 QUANTITATIVE RESULTS

The quantitative results on the CC3M and MS-COCO datasets (Table 5) indicate that APTP significantly outperforms the baseline Norm method in terms of FID and CLIP scores while also reducing complexity. For both datasets, APTP at 30k and 50k fine-tuning iterations shows lower FID and CMMD values and higher CLIP scores compared to the baseline, demonstrating the advantage of prompt based pruning compared to static pruning ideas for T2I models.

We also benchmark our method and the baselines on the PartiPrompt Yu et al. (2022) dataset using PickScore Kirstain et al. (2023). The prompts in this benchmark can be considered out-of-distribution for our model as many of them are significantly longer and semantically different from the ones in MSCOCO. We report the PickScore Kirstain et al. (2023) as a proxy for human preference and present the results in Table 2 below. We can observe that the PickScore of the pruned model is only 1% below the original Stable Diffusion 2.1, indicating that the pruned model can preserve the general knowledge and generation capabilities of the Stable Diffusion model. Table 6 demonstrates that

E.4.5 EXPERT ARCHITECTURES

Figures 11 and 12 display the block-level U-Net architecture of all experts of APTP-Base, with CC3M and COCO as the target datasets, respectively. The retained MAC patterns are markedly different, further corroborating that different datasets require distinct architectures and that a 'one-size-fits-all' approach is not well-suited for T2I models. For CC3M, down-sampling blocks generally are retained with higher ratios. Overall, APTP tends to prune Resnet Blocks more frequently and aggressively compared to Attention Blocks.

E.4.6 SAMPLES OF APTP

Table 7 displays the prompts for the images in Fig. 3 from CC3M and COCO validation sets.

We also provide more samples from APTP-Base pruned on CC3M and COCO. Fig. 13 presents samples from the validation set of CC3M generated by each 16 experts of APTP-Base at 0.85 MACs budget. Fig. 14 shows samples from the validation set of COCO from each of the 8 experts of APTP-Base pruned to 0.78 MACs budget.

1296
1297
1298
1299
1300
1301
1302
1303
1304
1305
1306
1307
1308
1309
1310
1311
1312
1313
1314
1315
1316
1317
1318
1319
1320
1321
1322
1323
1324
1325
1326
1327
1328
1329
1330
1331
1332
1333
1334
1335
1336
1337
1338
1339
1340
1341
1342
1343
1344
1345
1346
1347
1348
1349

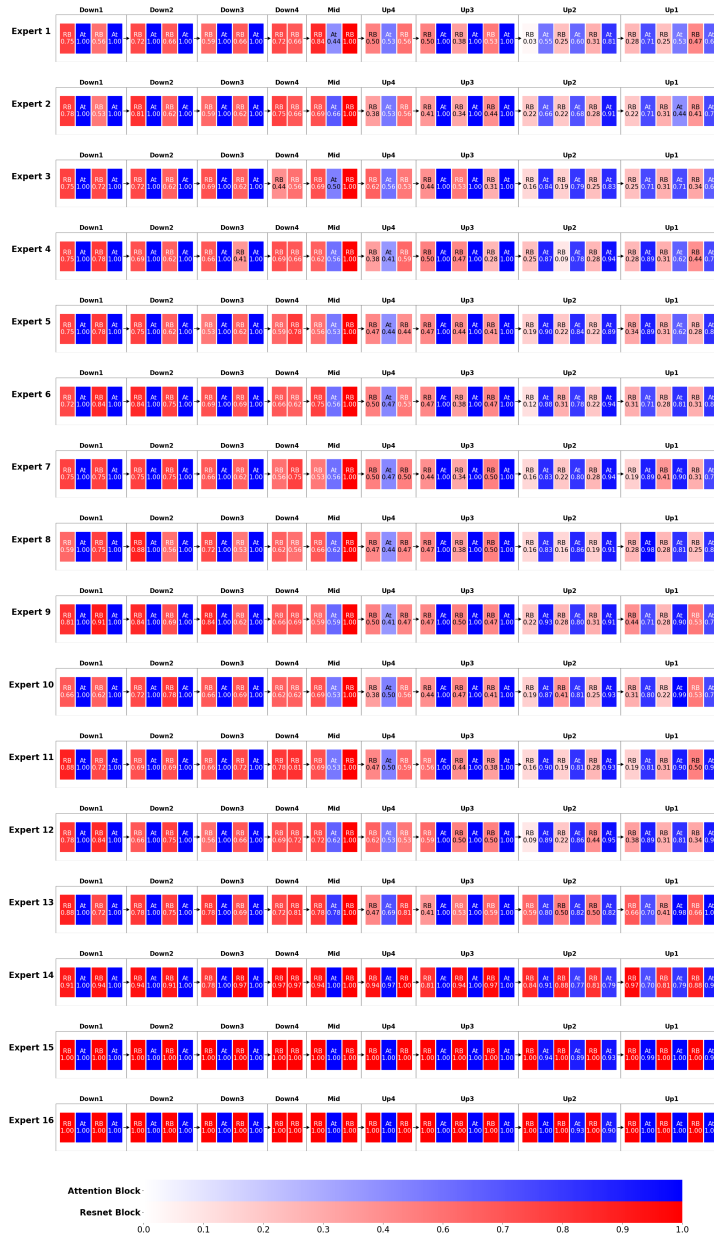


Figure 11: The block-level retained MAC ratio of the UNet architecture of all experts of APTP-Base applied to Stable Diffusion 2.1 with CC3M as the target dataset. The groups of ResBlocks and the heads of Attention Blocks are pruned based on the outputs of the architecture predictor. The intensity of the color of each block represents the resource utilization of it. The number in each block indicates the precise ratio of retained MACs of the block. Conv_in, Conv_out, and skip connections between corresponding down and up blocks are omitted for brevity.

1350
 1351
 1352
 1353
 1354
 1355
 1356
 1357
 1358
 1359
 1360
 1361
 1362
 1363
 1364
 1365
 1366
 1367
 1368
 1369
 1370
 1371
 1372
 1373
 1374
 1375
 1376
 1377
 1378
 1379
 1380
 1381
 1382
 1383
 1384
 1385
 1386
 1387
 1388
 1389
 1390
 1391
 1392
 1393
 1394
 1395
 1396
 1397
 1398
 1399
 1400
 1401
 1402
 1403



Figure 12: The block-level retained MAC ratio of the UNet architecture of all experts of APTP-Base applied to Stable Diffusion 2.1 with COCO as the target dataset. The groups of ResBlocks and the heads of Attention Blocks are pruned based on the outputs of the architecture predictor. The intensity of the color of each block represents the resource utilization of it. The number in each block indicates the precise ratio of retained MACs of the block. Conv_in, Conv_out, and skip connections between corresponding down and up blocks are omitted for brevity.

1458
1459
1460
1461
1462
1463
1464
1465
1466
1467
1468
1469
1470
1471
1472
1473
1474
1475
1476
1477
1478
1479
1480
1481
1482
1483
1484
1485
1486
1487
1488
1489
1490
1491
1492
1493
1494
1495
1496
1497
1498
1499
1500
1501
1502
1503
1504
1505
1506
1507
1508
1509
1510
1511

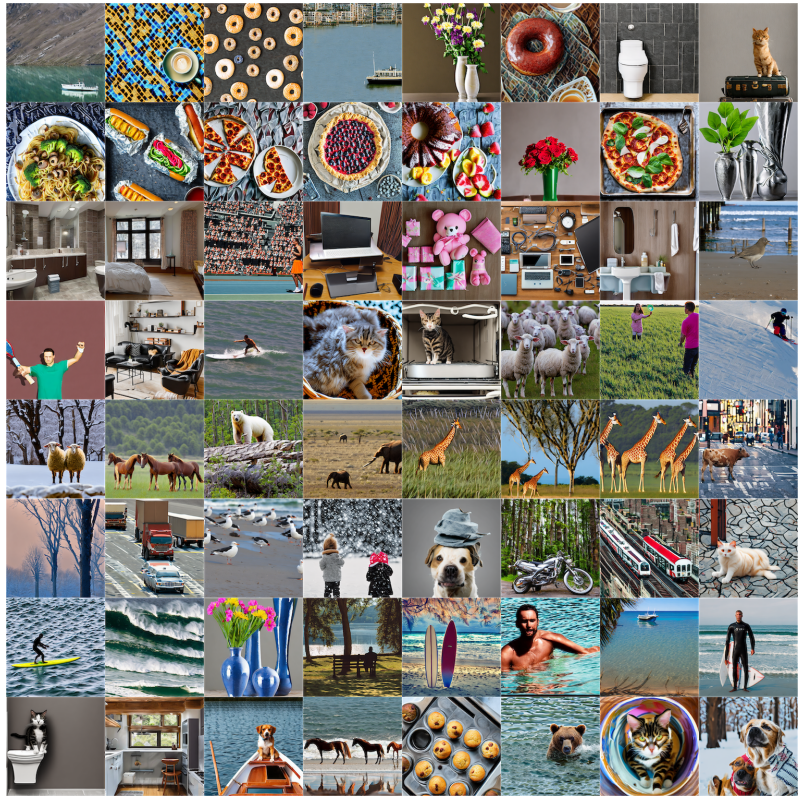


Figure 14: Samples of the APTP-Base experts after pruning the Stable Diffusion V2.1 using MS-COCO Lin et al. (2014) as the *target* dataset. Each row corresponds to a unique expert. Please refer to Table 4 for the groups of prompts assigned to each expert.

Table 5: Quantitative results on CC3M and MS-COCO. We report the performance metrics using samples generated at the resolution of 768 and downsampled to 256 Kim et al. (2023). We measure models’ MACs and Latency with the input resolution of 768 on an A100 GPU. @30/50k shows the model’s fine-tuning iterations after pruning.

CC3M						MS-COCO					
Method	Complexity		Performance			Method	Complexity		Performance		
	MACs (@768)	Latency (↓) (Sec/Sample) (@768)	FID (↓)	CLIP (↑)	CMMD (↓)		MACs (@768)	Latency (↓) (Sec/Sample) (@768)	FID (↓)	CLIP (↑)	CMMD (↓)
Norm Li et al. (2017) @30k	1185.3G	3.4	157.51	26.23	1.778	Norm Li et al. (2017) @30k	1077.4G	3.1	60.42	27.06	1.524
Norm Li et al. (2017) @50k	1185.3G	3.4	141.04	26.51	1.646	Norm Li et al. (2017) @50k	1077.4G	3.1	47.35	28.51	1.136
APTP(0.66) @30k	916.3G	2.6	60.04	28.64	1.094	APTP(0.64) @30k	890.0G	2.5	39.12	29.98	0.867
APTP(0.66) @50k	916.3G	2.6	54.95	29.08	1.017	APTP(0.64) @50k	890.0G	2.5	36.17	30.21	0.739
APTP(0.85) @30k	1182.8G	3.4	36.77	30.84	0.675	APTP(0.78) @30k	1076.6G	3.1	22.60	31.32	0.569
APTP(0.85) @50k	1182.8G	3.4	36.09	30.90	0.669	APTP(0.78) @50k	1076.6G	3.1	22.26	31.38	0.561
SD 2.1	1384.2G	4.0	32.08	31.12	0.567	SD 2.1	1384.2G	4.0	15.47	31.33	0.500

(a)

(b)

Table 6: Results on PartiPrompts. We report performance metrics using samples generated at the resolution of 768. We measure models’ MACs/Latency with the input resolution of 768 on an A100 GPU. @30/50k shows fine-tuning iterations after pruning.

Train on CC3M				Train on MS-COCO			
Method	Complexity		PartiPrompts PickScore (↑)	Method	Complexity		PartiPrompts PickScore (↑)
	MACs (@768)	Latency (↓) (Sec/Sample) (@768)			MACs (@768)	Latency (↓) (Sec/Sample) (@768)	
Norm (Li et al., 2017) @50k	1185.3G	3.4	18.114	Norm (Li et al., 2017) @50k	1077.4G	3.1	18.563
SP (Fang et al., 2023) @30k	1192.1G	3.5	18.727	SP (Fang et al., 2023) @30k	1071.4G	3.3	19.317
BKSDM (Kim et al., 2023) @30k	1180.0G	3.3	19.491	BKSDM (Kim et al., 2023) @30k	1085.4G	3.1	19.941
APTP(0.66) @30k	916.3G	2.6	19.597	APTP(0.64) @30k	890.0G	2.5	20.626
APTP(0.85) @30k	1182.8G	3.4	21.049	APTP(0.78) @30k	1076.6G	3.1	21.150
SD 2.1	1384.2G	4.0	21.316	SD 2.1	1384.2G	4.0	21.316

(a)

(b)

1566
1567
1568
1569
1570
1571
1572
1573
1574
1575
1576

CC3M Prompts

1578 Saw this beautiful sky on my way home.
1579 A silhouetted palm tree with boat tied to it rests on a beach that a man walks across during golden hour.
1580 Sketch of a retro photo camera drawn by hand on a white background.
1581 From left: person person, the dress on display.
1582 Never saw a doll like this before but she sure is sweet looking.
1583 The team on the summit.
1584 A water drop falls towards a splash already made by another water drop.
1585 Husky dog in a new year's interior.
1586 Old paper with a picture of flowers, ranked in a moist environment.
1587 People on new year's eve!
1588 I drive over stuff - a pretty cool jeep, 4x4, or truck t-shirt.
1589 The crowds arrive for day of festival.
1590 A scary abandoned house under a starry sky.
1591 Freehand fashion illustration with a lady with decorative hair.
1592 Introduce some new flavors to your favorite finger food with these inspired chicken wings.
1593 Gloomy face of a sad woman looking down, zoom in, gray background.

COCO Prompts

1594 A white plate topped with a piece of chocolate covered cake.
1595 Decorated coffee cup and knife sitting on a patterned surface.
1596 A desk topped with a laptop computer and speakers.
1597 A man sitting on the beach behind his surfboard.
1598 A pizza type dish with vegetables and a lemon wedge.
1599 The browned cracked crust of a baked berry pie.
1600 A tennis player in an orange skirt walks off the court.
1601 The skier in the helmet moves through thick snow.
1602 A giraffe walks leisurely through the tall grass.
1603 Several brown horses are standing in a field.
1604 A red fire hydrant on a concrete block.
1605 A bus driving in a city area with traffic signs.
1606 There is a man on a surf board in the ocean.
1607 A boat parked on top of a beach in crystal blue water.
1608 A small kitchen with low a ceiling.
1609 A calico cat curls up inside a bowl to sleep.

Table 7: Prompts for Fig. 3

1610
1611
1612
1613
1614
1615
1616
1617
1618
1619

1620
1621
1622
1623
1624
1625
1626
1627
1628
1629
1630
1631
1632
1633
1634
1635
1636
1637
1638
1639
1640
1641
1642
1643
1644
1645
1646
1647
1648
1649
1650
1651
1652
1653
1654
1655
1656
1657
1658
1659
1660
1661
1662
1663
1664
1665
1666
1667
1668
1669
1670
1671
1672
1673

Prompts

- a trash bin
 - a woman with sunglasses and red hair
 - a close-up of an ostrich’s face
 - a black t-shirt
 - A helicopter flies over Yosemite.
 - a spaceship hovering over The Alamo
 - a corgi
 - A bar of chocolate without a wrapper that has the word "WRAPPER" printed on it.
 - a laptop screen showing a bunch of photographs
 - a street
 - a handpalm with leaves growing from it
 - a close-up of the keys of a piano
 - the Eiffel Tower in a desert
 - a view of the Earth from the moon
 - the silhouette of the Millenium Wheel at dusk
 - an avocado on a table
 - a glass of orange juice to the right of a plate with buttered toast on it
 - a Styracosaurus
 - view of a clock tower from below
 - a hat
-

Table 8: Prompts for Fig. 7